Assignment and Extracting Dynamics from Experimentally and Theoretically Obtained Spectroscopic Hamiltonians in the Complex Spectral and Classically Chaotic Regions

Christof Jung*

Instituto de Ciencias Fisicas, Universidad Nacional Autonoma de Mexico, Av. Universidad s/n, 62251 Cuernavaca, Mexico

Howard S. Taylor

Department of Chemistry, University of Southern California, Los Angeles, California 90089

Received: October 13, 2006; In Final Form: January 17, 2007

An analysis of existing algebraic multiresonance spectroscopic Hamiltonians, derived by fitting to experimental data or from classical canonical or quantum Van Vleck perturbation theory, allows without any significant further classical or quantum calculation the assignment of quantum numbers and motions to states observed in spectra that were previously thought to be irregular or just unassignable. In such cases, inspection of the amplitude and phase of eigenfunctions previously calculated in the Hamiltonians derivation process but now transformed to a reduced dimension semiclassical action−angle representation reveals extremely simple albeit unfamiliar topologies that give quantum numbers by simply counting nodes and phase advances. The topology allows these simple wave functions to be sorted into dynamically different excitation ladders or classes of states which are associated with different regions of phase space. The rungs of these ladders or the states in the classes intersperse in energy causing the spectral complexity. No experimental procedure allows such sorting. The success of the work stems from (1) the qualitative insights of nonlinear dynamics, (2) the conversion of the quantum problem in full dimension to a semiclassical one in reduced dimension by use of a canonical transform that takes advantage of the polyad and other constants of the motion, and (3) the judicious choice of the reduced angle variables to reflect rational ratio resonance frequency conditions. This leads to localization of those semiclassical wave functions, which are affected by the particular resonance. In reverse, the localized appearance of the reduced dimension wave function reveals which resonances govern it and makes sorting visually simple. The success of the work also stems from (4) the revealing use of plots of phase advances as well as the usual densities of the eigenstates for sorting and assignment purposes. Even in classically chaotic regions, organizing trajectories, which correspond to averages over regional phase space structures that need not be computed, can easily be drawn as the structure about which eigenfunction localization takes place. The organizing trajectories when transformed back to the full dimensional configuration space reveal the internal molecular motions. The complexity of the usual quantum stationary and propagated wave functions and associated classical trajectories forbids most often such assignments and sorting. This procedure brings the ability to interpret complex vibrational spectra to a degree previously thought possible only for lower excitations. The new methodology replaces and extends the computationally more difficult parts of a procedure used by the authors that was applied successfully to several molecules during the past few years. The new methodology is applied to DCO, CHBrClF, and the bending of acetylene.

1. Introduction and Overview

In recent years, significant progress has been made in interpreting and assigning measured dispersed fluorescence and Fourier transform (FT) IR electronic ground state vibrational spectra for small molecules such as C_2H_2 (the bending spectrum),[1−6] CHBrClF,[7,8] DCO,[9,10] CDBrClF,[11,12] CF$_3$CHFI,[13,14] and SCCl$_2$.[15,16] These molecules had what was deemed complex, perhaps even uninterpretable, spectra in the high vibrational region. Ideally, we would like to be lead in our interpretations by what was done in the low vibrational region.[17] We would thus like to extract several types of information from the experiments or from a theoretical quantum chemical calculation of the energies and wave functions that underlie the spectra observed in the experiments: first, a listing of the types of vibrational interactions that influenced these levels; second, a

resulting dynamical model whose quantization leads to the levels probed in the experiment; and third, an assignment for these levels in terms of quasiconstants of the motion in a number equal to the number D of degrees of freedom of the system.

Unfortunately, except for specifying the interactions, the well-known methods[17] used successfully at a lower excitation to achieve these aims failed in the complex spectral region. These methods essentially used perturbation theory that started with a normal or local mode model. Convergence to a satisfactory result was possible if upon excitation the model motions were perturbed by the anharmonicity into continuous distortions of themselves. The case of a single dynamical resonance (e.g., Fermi, Darling Denison, etc.) where combinations of effective frequencies, that is, fundamentals altered by anharmonic effects, came into a rational ratio could also be treated as the system was still dynamically regular, and essentially, degenerate

perturbation theory could be used to treat the levels in the spectral region where the single resonance was active.

Complex spectra have more than one dynamical resonance meaning that perturbation theory would fail and chaos was possible. Also, unlike the low excitation region, in the complex region even when quantum chemically calculated or empirically fitted potential surfaces did exist and advanced calculational methods[18−21] could be used to yield configuration space represented eigenfunctions and propagated wave packets, they were often too complex in topology and too high in spatial dimension to aid in the spectral interpretation. Some papers could extract dynamics of the lowest and highest states in the polyad[22] and perhaps a few intermediate states; however, generically no nodal loci or planes could be observed, and no definitive decisions could be made about classical motions or assignments although energy flow could be tracked.[8,12,14,16] Full or reduced dimensional wave function density plots that might rarely reveal a simple nodal pattern existing in a now understandable wave function shape most often failed to aid in the interpretation of other far away or even close by states. Different states seemed to need different slices and projections, and for many states, slices and projections did not reveal a systematic underlying dynamically based assignment.

For complex spectra, the analysis of the spectral data was most often fit to multiresonant effective algebraic Hamiltonians H_{eff} and was given along with its eigenfunctions in the normal mode number representation. Alternatively, the data were often fit[8,16] to a potential hypersurface for further quantum calculational use or for processing by means of quantum Van Vleck perturbation theory[23] or classical Birkhoff−Gustavson perturbation theory[24,25] into an H_{eff} and the associated constants of the motion called the polyad quantum numbers. In the fitted H_{eff} case, the constants or any linearly independent mixture of them could be obtained most efficiently by using the vector model developed by Kellman[26] and Ezra and Fried.[24] It was always possible to make such linear combinations where one of these constants of the motion could be taken to represent a total excitation quantum number (say in units of the lowest mode frequency) for the polyad. Other combinations depending on the problem could be recognized as, say, conservation of bending angular momentum and other conserved quantities. Recall that the polyad numbers which break the problem into ones parametric in the specific values of these conserved quantities only tell the totality of excitation or angular momentum but not its distribution among the various motions underlying a particular state of excitation. This means that in one polyad the states could be still quantized on a complex variety of underlying dynamics.

The quantum $H_{\text{eff}}(a^{\dagger}, a)$ is algebraic and given in terms of creation and destruction operators. The classical $H_{\text{eff}}(I, \phi)$ being the classical limit of the quantum H_{eff} is given in terms of action and angle variables (I, ϕ) and related by Heisenbergs correspondence relations[27]

$$a_j \rightarrow \sqrt{I_j} \exp(i\phi_j) \qquad a_j^{\dagger} \rightarrow \sqrt{I_j} \exp(-i\phi_j) \qquad (1)$$

Here and in the following, if we write a or I or any other multicomponent variables without any index, then we mean the complete set of all components of this variable. The resulting even high order actions were taken as indicated by the results of perturbation theory as close to harmonic oscillator forms,[25] even when fitted H_{eff} was used and the actions were in principle abstract. Confidence in this harmonic association is gained by substituting for the normal mode number representation basis functions appearing in the eigenstates the normal mode harmonic

basis functions in the normal coordinates.[23] These eigenfunctions based on $H_{\text{eff}}(a^{\dagger}, a)$ were then compared to those obtained by diagonalizing the configuration space Hamiltonian on the latter basis. The results compare qualitatively, and the state-by-state association is clearly recognizable.[23]

The great achievement of the spectral Hamiltonian not only was the reduction of the content of spectral tables and graphs to a dynamical form but also was the uncovering of the types of interactions that influenced the system.[5,8,12,14] Another achievement was to make the assignment problem simpler as the values of the polyads were themselves quantum numbers for the states in the polyad. This reduces the number of to be assigned quantum numbers to the number of degrees of freedom, D, minus the number of polyad quantum numbers F. This in turn suggests that the problem could be reduced to one involving just this number of variables. This was done by many groups for model systems[28,29] for single resonance regular systems such as HOCl, HCP, CO_2, and others and for multiresonance systems by Sibert and McCoy[30] and by Ezra and Fried[24] employing a canonical transformation to replace F actions by the polyad quantum numbers, thereby making cyclic their conjugate angles and creating a more visually representable and dynamically simpler, reduced dynamics, albeit still a multiresonant problem. Sibert and McCoy also showed in the acetylene bending mode problem that the eigenfunctions of the reduced dimension Hamiltonian $H_{\text{eff}}(J, \psi)$ could be calculated and their density exhibited in angle space ψ. The eigenfunctions were now represented in the reduced dimension semiclassical analogue of the number basis.

In spite of all this progress for the multiresonant case, no fully successful assignment or dynamic models appeared. Several at least partially successful nonlinear classical approaches for molecules as water appeared.[31−35] These latter methods required the use of significant nonlinear classical computation and a rather deep grasp of the ideas of nonlinear dynamics. It was at this point that the present authors introduced several new ideas that in their simplest version enabled the remaining task to be accomplished by analysis, the computer being needed only for graphics. The words "simplest version" are used in admission of the fact that our earliest papers, while totally correct in results, could have been made simpler by the now existing present methodology, which eliminates the complicated, both computationally and visually, process of first searching the reduced dimension phase space for the periodic orbits or lower dimensional tori, called organizing structures, about which the ultimately uncovered motions would move. Our later equivalent methodology introduced several new ideas such as choosing the new angle variables ψ in the canonical transformation so as to stop it from changing values if and when the studied eigenfunction is influenced heavily by a particular resonance. As the classical motion now hovered about these values of ψ, the wave function of this eigenstate was localized similarly. This simultaneously simplified the visual representation of most of the eigenfunctions and allowed visual recognition to enable the sorting of the wave functions into classes or ladders of states dominated by the same, now identifiable, sets of resonances associated with the fixed variables. This visual inspection was made easier by the realization that these, now angle space wave functions, were inherently complex (as opposed to real) functions. They often allowed revealing information to be obtained not only from the density plots but also from phase plots as well. The latter showed similar patterns for functions dominated by the same resonances. In a playing

TABLE 1: Resonant Interaction Terms in the Various Molecules Mentioned in the Main Text[a]

name	D	F	j	$\vec{r}_j$	k_j	name	D	F	j	$\vec{r}_j$	k_j
DCO	3	1		m,n,b		CDBrClF	4	1		s,f,a,b	
			1	(1,0,−2)	14.6				7	(0,2,−2,0)	−0.8
			2	(0,1,−2)	−4				8	(0,2,0,−2)	2
			3	(1,−1,0)	42.3				9	(0,0,2,−2)	−0.6
			4	(2,−2,0)	−3.4	CF$_3$CHFI	4	1		s,f,a,b	
CHBrClF	3	1		s,a,b					1	(1,−2,0,0)	14.7
			1	(1,−2,0)	31.8				2	(1,0,−2,0)	23.5
			2	(1,0,−2)	40.4				3	(1.0,0,−2)	19.7
			3	(1,−1,−1)	7.5				4	(1,−1,−1,0)	22.1
			4	(0,2,−2)	−5.5				5	(1,−1,0,−1)	7.4
C$_2$H$_2$	4	2		$4_d, 4_g, 5_d, 5_g$					6	(1,0,−1,−1)	6.3
			1	(1,1,−1,−1)	−8.6				7	(0,2,−2,0)	−7.6
			2	(−1,1,1,−1)	−6.2				8	(0,2,0,−2)	−13.3
			3	(2,0,−2,0)	1.8				9	(0,0,2,−2)	−10.5
			4	(0,2,0,−2)	1.8	SCCl$_2$	6	3		1,2,3,4,5,6	
CDBrClF	4	1		s,f,a,b					1	(1,0,0,0,−1,−1)	−10
			1	(1,−2,0,0)	18.1				2	(0,−1,0,0,1,−1)	−10.9
			2	(1,0,−2,0)	14.1				3	(1,−1,−2,0,0,0)	0.05
			3	(1,0,0,−2)	21.4				4	(1,−1,0,0,0,−2)	−0.05
			4	(1,−1,−1,0)	34.3				5	(1,1,0,0,−2,0)	4.1
			5	(1,−1,0,−1)	−32.6				6	(0,0,2,0,0,−2)	−0.82
			6	(1,0,−1,−1)	32.8						

[a] First column gives the name of the molecule. The second column gives the number of degrees of freedom. The third column gives the number of independent conserved quantities. The forth column gives the number j of the resonance vector $\vec{r}(j)$ in the Hamiltonian. The fifth column gives in the first row the labels we give to the various degrees of freedom and in the rows below the corresponding resonance vectors $\vec{r}(j)$ from eq 5 themselves in this order of degrees of freedom. The sixth column gives the numerical value of the strength parameter of the resonant interactions in lowest order; higher order corrections to k are not included.

card analogy, each state is now one card with density on one side and the phase plot on the other side.

The localization enabled the simple visualization of idealized organizing structures which were actual fundamental dynamical motions and which could be transformed backward to (I, ϕ) and on to the original mode variables. This allowed, if the initial dimension were not too great, the observation of the new motions in analogy to that done at low excitation. This process was called the "lift''.

From the eigenstate graphics for most states, nodes could be seen in the density diagram and phase advances in the phase diagrams which acted as the values of the residual quantum numbers completing the assignment and allowing a rung ordering of the states. The ladders of which several could coexist in energy in a given polyad and which lay in phase space in different resonance zones were now analogous to suites in a deck of cards, and the origin of spectral complexity was revealed. Nature had shuffled the deck while giving, even within one polyad, the experimentalist no tool to sort the suites. Our methodology supplies the tool.

The effective Hamiltonian can only be derived and a unique set of action and angle variables can be obtained for states in a system where motion is confined to a single well. If barriers exist, then the result can be useful below the barrier for all states but can also be useful above the barrier or even at or above the dissociation limit (e.g., DCO) where analogues of true resonances remain localized above a single well. When barriers and tunneling exist at low energy, as in water, the H_{eff} and therefore the whole method is ill-defined. The method will also be difficult to implement when $D - F > 3$. Here, presently, visualization of wave functions is simply too difficult as is the search for classical organizing structures.

This review was written to present the simplest "no computation" analysis version of the theory. It starts by assuming an H_{eff} and the eigenfunctions in each polyad in the number representation to be available, as is most often the case. The latter are easily obtained but do need a computer to do so. Another purpose is to enable a non-theorist to implement the

analysis without fully appreciating nonlinear dynamics. This review was not written to represent all the results given in our previous publications. Examples of the analysis from our papers or improvements of such will be used to illustrate the points made in the subsections and will be appropriately placed. The acetylene analysis used here as an example presents a simpler methodology leading to a more revealing alternative assignment than previously given.

2. Hamiltonian

From hereon, it will be assumed that either $H_{\text{eff}}(a^\dagger, a)$ or its classical correspondence limit $H_{\text{eff}}(I, \phi)$ is available. They are related by eq 1. Since, as will be seen, the plots of the wave functions will ultimately be most simple when represented in angle configuration space, here, we assume one starts with or has transformed $H_{\text{eff}}(a^\dagger, a)$ to $H_{\text{eff}}(I, \phi)$ whose resonance contributions we show in Table 1 for each of the systems we have studied. It contains parameters that are plugged into the generic form

$$H_{\text{eff}}(I, \phi) = H_0(I) + W(I, \phi) \tag{2}$$

where

$$H_0(I) = \sum_{j=1}^{N} \omega_j I_j + \sum_{j \leq n} x_{j,n} I_j I_n + ... \tag{3}$$

The dots mean that any higher order anharmonicities can be included

$$W = \sum_{\vec{r}} k_{\vec{r}} [\prod_{n=1}^{D} I_n^{|r_n|/2}] 2 \cos(\sum_{n=1}^{D} r_n \phi_n) \tag{4}$$

Here, the components of the vector $\vec{r}$ are integers; below it will be explained which values for $\vec{r}$ actually are included in the sum.

3050 *J. Phys. Chem. A, Vol. 111, No. 16, 2007*

Jung and Taylor

Here, H_0 contains the harmonic first terms plus the anharmonicity terms (whose parameter values are in the original sources[6,8,10,12,14,15]) and is diagonal in the number representation. W contains the resonances. Table 1 gives the jth resonance by specifying the vector $\vec{r}^{(j)}$ with components $r_n^{(j)}$ such that it corresponds to the term in W with

$$\sum_{n=1}^{D} r_n^{(j)} \phi_n = \vec{r}^{(j)} \cdot \vec{\phi} \tag{5}$$

as the argument of its cosine function. Here, $\vec{\phi}$ is the vector with components being the angles ϕ_n. Importantly, note that, using $\omega_n = d\phi_n/dt$, $d(\vec{r}^{(j)} \cdot \vec{\phi})/dt = \vec{r}^{(j)} \cdot \vec{\omega} = 0$ is the jth resonance condition. The $\vec{r}$ values in the sum should then be the $\vec{r}^{(j)}$ as only then are the effects of the cosine terms maximized when the system is in the region of phase space where the resonance is important.

Having the $\vec{r}$ vectors, the constants of the motion can be obtained using Kellman's and Ezra and Fried's vector models[24,26] as follows. Consider the space R spanned by all vectors $\vec{r}^{(j)}$, and determine its dimension, called N. Construct a set of $D - N = F$ vectors $\vec{s}^{(j)}$, $j = 1, ..., F$ that serve as a basis for the orthogonal complimentary space S. The F independent constants of motion are then

$$K_j = \vec{s}^{(j)} \cdot \vec{I} \tag{6}$$

with the vector $\vec{I}$ being the vector whose components are the actions I_n. Note that different choices of the S basis lead to different polyad constants although all choices are linear combinations of the ones resulting from other choices. We have found the choice, that minimizes the norm of the $\vec{s}$ vectors, convenient in the sense of later being able to recognize more easily variables whose motion is associated with particular resonances. The physics does not require this last step.

Often the K_j or some of them are chosen as functions of I that correspond to physically motivated conservations. Examples are the total excitation or polyad, used in almost all the systems we deal with, and the conservation of bending angular momentum as in the acetylene case. This implicitly chooses an S space basis.

The polyad constants of the motion given in the literature often appear in the number representation and can be converted to the corresponding classical action representation using for mode k

$$n_k = I_k - 1/2 \tag{7}$$

For any constant of the motion, we can add or leave out constant terms when convenient.

The ultimate derived dynamics is qualitatively robust with respect to small quantitative changes in the potential from which it is derived. This is because the effective Hamiltonian omits higher order presumably small effects and small resonances. This is why, when wave functions in normal coordinates are constructed from the eigenstates of $H_{\text{eff}}(a^\dagger, a)$ in the number representation by replacing $|n_j\rangle$ by the n_jth harmonic normal mode eigenstate in terms of the variable q, that the resulting functions look like an idealized undistorted and "nonjittering" version of the eigenstates of $H(p, q)$.

3. *D* Dimensional Action Angle Representation

The configuration space now is that of the angles ϕ_k, $k = 1, ..., D$ and as such is a D dimensional torus T^D defined by the D

fundamental loops; that is, it is a Cartesian product of the D fundamental loops over which a particular ϕ_k varies from 0 to 2π. Wishing to represent the eigenfunctions, so far, given in the number representation in the ϕ space before transformation to a lower N dimensional space, it is required to express any number basis function as a function of ϕ. As the number basis are the eigenfunctions of the nonresonant part of H_{eff}, the eigenfunctions of $H_0(I, \phi)$ are taken as a basis. Using the Schroedinger quantization scheme, we found this basis function is of periodic plane wave form on the angle torus, namely,

$$\chi_n(\phi) = \exp(in\phi) \tag{8}$$

Here, we recall the convention that n and ϕ without any index are D dimensional vectors, and in the argument of the exponential function, we have the scalar product of these vectors. The vector n specifies the number basis state corresponding to χ_n. χ_n, when examined along a fundamental loop associated with varying ϕ_j holding all other ϕ_k constant, exhibits a phase advance of $n_j 2\pi$; that is, n_j can be determined by such an examination, a process that will be extensively employed later.

The expansion of the eigenstates of $H(a^\dagger, a)$ into number states as it comes out of the diagonalization translates into the expansion of the wave function into periodic plane waves from eq 8 on the configuration torus. That is, it translates into the Fourier decomposition of the wave function on the torus. Specifically, the eigenfunction corresponds as

$$|\Psi_k\rangle = \sum_{n \in \text{polyad}} c_{k,n} |n\rangle \rightarrow \sum_{n \in \text{polyad}} c_{k,n} \chi_n(\phi) = \Psi_k(\phi) = \langle \phi | \Psi_k \rangle \tag{9}$$

The reader should note that up to here, since the $c_{k,n}$ vector was given, one only needs to trivially plug in the $c_{k,n}$ into eq 9 to get started with the analysis. Equation 9 shows that the eigenstates are inherently complex, meaning that one should study their phase as well as the usual magnitude.

The replacement in eq 9 of the n basis by the $\chi_n(\phi)$ basis is why eq 9 is called a "semiclassical" eigenfunction. It is valid to order $\hbar$.

4. Transformation to Reduced dimension Variables

As discussed in section 1, a canonical transformation, which is most simple when using action/angle variables, is used to transform from the (I, ϕ) variables in D dimensions to an effective $N = D - F$ dimensional space. We say "effective" because the transformation will connect the D dimensional (I, ϕ) problem to the D dimensional (J, ψ) variables in such a way that $F = D - N$ of the new actions will each be equal to one of the known (from section 2) polyad expressions as a function of I leaving an N variable problem. As such, to carry out the canonical transformation, we are free to choose the new actions as

$$J_k = I_k \quad k = 1, ..., N$$

$$J_{N+l} = K_l \quad l = 1, ..., F \tag{10}$$

which in $D \times D$ dimensional matrix notation, since K_j depends on the I_n, is defined by

$$J = MI \tag{11}$$

The choice of the first N lines is done for the sake of having, later in the analysis, simple interpretations. The last F lines will ensure that the new angles ψ_k conjugate to the constant actions

will be cyclic. Hence, the transformed Hamiltonian can now be written as $H_{eff}(J_1, ..., J_N; \psi_1, ..., \psi_N; K_1, ..., K_F)$. Therefore, one can now work separately in each polyad specified by $K_1, ..., K_F$. The effective configuration space dimension, that is the reduced dimension, is now N. The reduced configuration angle space is now an N dimensional torus T^N with its own fundamental loops and phase advances.

To determine the transformation from the ϕ_j to the ψ_j, a generator function

$$G(I, \psi) = \sum_{k=1}^{D} \psi_k J_k = \psi^T M I \qquad (12)$$

is used. The new actions are then

$$J_k = \partial G/\partial \psi_k = J_k(I) \qquad (13)$$

and as such remain as in eq 10. The new angles are solved from the equations for ϕ in terms of ψ as

$$\phi_l = \partial G(I, \psi)/\partial I_l = \sum_{k=1}^{D} [\partial J_k(I)/\partial I_l]\psi_k$$

or

$$\phi = M^T \psi \qquad (14)$$

the derivatives being available from eq 12, whose dependence on the I is determined by the choice of the compliment space basis $\vec{s}^{(j)}$. M allows for the matrix form of these equations. The solution, since M is invertible due to the fact that all R and S space basis vectors were linearly independent, is

$$\psi = (M^{-1})^T \phi \qquad (15)$$

Clearly, there are two places where we have freedom in defining the J which in turn determines the ψ_k, $k = 1, ..., N$ angles of the configuration torus in reduced space and the F cyclic angles, denoted hereafter by θ_{N+l}, $l = 1, ..., F$. The first choice is to which of the original modes each of the first N values of I should correspond. The second is whether to use the F constants of the motion given by the experimentalists or some linear combination of them. For the latter choice, we have decided to retain the physically motivated choices made by the experimentalists. For DCO and CHBrClF, there was in fact no choice at all since $F = 1$. In DCO, we took I_1 and I_2 to be the two stretches, and for CHBrClF, we took them to be the two bends of the hydrogen atom. For acetylene to remain consistent with ref 1 for the first two J_k, we took them, not as in eq 10, to be particular linear combinations of the four I_k taken in ref 1. We thereby avoided a difference in the formulas between this paper and ref 1. By these choices in all of these examples, the ψ_k are now given in terms of the ϕ as

$$\psi_j = \vec{r}^{(j)} \cdot \vec{\phi} \qquad (16)$$

where the N vectors $\vec{r}^{(j)}$ are each associated with one of the resonances in the Hamiltonian.

In a resonance region, a classical resonance then leads to classical localization which in turn leads to quantum localization. To see this, consider an ensemble of trajectories governed by $H(J, \psi; K)$ that are localized in some or all of the ψ variables on the surface of an N dimensional toroidal configuration space T^N. Then, let ψ be equal to its average value inside the region. With this, it is assured that the trajectories so localized are

subject to phase and frequency locking. Phase locking means that these averages do not change, even slowly over time, and that the ϕ in the definition of the ψ represents motions that are locked in phase.

Observed classical localizations can be used to determine the particular resonances causing the localization. That is, since each localized ψ_j is approximately a fixed constant in the region, then by eq 16, we get $d\psi_j/dt = \vec{r}^{(j)} d\phi/dt = \vec{r}^{(j)} \cdot \omega = 0$. This last relation points to the jth resonance as causing the localization of ψ_j and explains why the ψ_j, $j = 1, ..., N$ are often called the slow variables.

The localization semiclassically translates to quantum wave functions also being similarly localized, a feature which is easily noted by visual inspection. Observing in which ψ_j a quantum eigenstate density is localized then reveals which resonances are determining its localization. Grouping eigenfunctions by similar localizations of density or phase advances under the density then forms the classes or ladders of states referred to in section 1. Depending on D and the number of active resonances, we find the fixed values of the localized ψ determine points, lines, planes, etc. about which the wave function is organized. These organizing features approximate actual phase space structures that actually can then be transformed back to (I, ϕ) space and then on to displacement space if it is assumed that displacements and the action angle variables are harmonically related. This process is called the lift and is presented in detail in section 7. The lift determines the idealized motion of the molecule in displacement space which when quantized leads to eigenstates in the ladders or classes formed by similar localization.

5. Reduced Space Polyad Specific Eigenfunctions

The basis functions $\chi_n(\phi)$ in eq 8 can now be transformed to the new ψ variables. Using $I_j = n_j + 1/2$, apply eq 14 to the ϕ in eq 8 and get

$$\vec{\phi}\vec{n} = \vec{\psi}M\vec{n} \qquad (17)$$

Define $\vec{p} = M\vec{n}$ so that $\vec{\phi}\vec{n} = \vec{\psi}\vec{p}$. Note that the last F components of $\vec{p}$ and $\vec{\psi}$ are constants and cyclic angles respectively and the first N are the first occupation numbers in state $|n\rangle$. Inserting this into eq 8 gives

$$\exp(in\phi) = \exp[i(K_1\psi_{N+1} + ... + K_F\psi_{N+F})] \times \\ \exp[i(p_1\psi_1 + ... + p_N\psi_N)] \quad (18)$$

As such,

$$\chi_n(\phi) \rightarrow \chi_n(\psi) = \exp[i(p_1\psi_1 + ... + p_N\psi_N)] \qquad (19)$$

and by eq 9

$$\Psi_k(\phi) \rightarrow \Psi_k(\psi) = \sum_{p \in polyad} c_{k,p} \exp[i(p_1\psi_1 + ... + p_N\psi_N)] \qquad (20)$$

where the common global phase factor, constant over the polyad, has been dropped from all basis functions as it cannot help distinguish any physics among the functions in the polyad. All eigenfunctions are now reduced to be functions of ψ_k, $k = 1, ..., N \leq D$.

At this stage of the analysis, the only actual work, as opposed to discussion, is (i) to write eq 20 with the system dependent numbers $c_{k,p}$ from the diagonalization of $H_{eff}(a^\dagger, a)$ in the number basis, (ii) to use simple algebra in the vector model to get the constants of the motion in eq 6, and (iii) to recognize M in eq
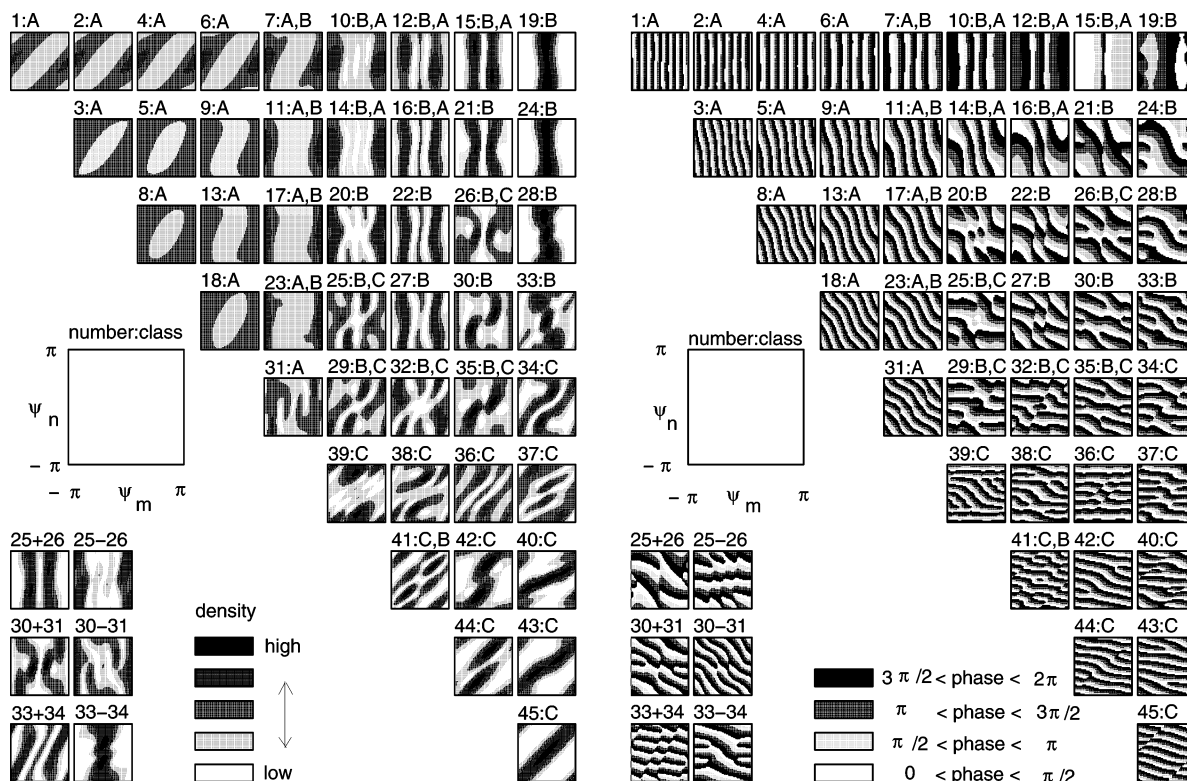
Figure 1. Part a shows the density of the semiclassical wave functions of all 45 eigenstates of polyad 8 of DCO plotted on the toroidal configuration space cut open. The horizontal coordinate ψ_m and the vertical coordinate ψ_n both range from $-\pi$ to π. Darker gray means higher density. Each little frame is labeled above by the number of the state and by the class or sometimes several classes into which this state is sorted according to Table 2. Part b shows in exactly the same arrangement the phases of the wave functions. Here, white means phase in the interval $[0, \pi/2)$, light gray means phase in the interval $[\pi/2, \pi)$, dark gray means phase in the interval $[\pi, 3\pi/2)$, and black means phase in the interval $[3\pi/2, 2\pi)$. In the left lower corner, some additional little frames show the results of demixing for some states.

11 to get the ψ_j, $j = 1, ..., N$ and the F cyclic angles ψ_j, $j = N + 1, ..., D$ and to recognize the vector $\vec{p}$. For DCO and CHBrClF, where eq 10 is used, the first N components p_j are the first N occupation numbers, respectively. For acetylene, J_k will be a linear combination of I_j, $j = 1, 2, 3, 4$, and p_k will be the same linear combination of the first N occupation numbers.

Clearly, each eigenfunction is now available for graphical representation in reduced dimension space. Plotting its density and phase on the surface of a T^N torus is clearly not practical. In fact, what we now do is really only practicable for problems with $N < 4$. We imagine representing the torus T^N as an N dimensional cube with identified opposite boundary points. A point on any of the cubes boundaries corresponds to one in a similar position on the opposite boundary. This is just the N dimensional generalization of a point on a rolling circle being able to be represented on a graph with the angle varying from 0 to 2π but with enforced periodic boundary conditions. An N dimensional torus T^N is a Cartesian product of N rings thereby implying an N dimensional cube with identified opposite boundary points and edges measuring an angle ψ_j spanning a range of 2π. For simplicity here, only problems with $N = 2$ will be chosen.

Therefore, in this paper, we plot the density and the phase of the eigenfunctions on two-dimensional squares with angles ranging over 2π. The angle at the center of the angle range is chosen by trial and error to give a more revealing picture that minimizes various features that are symmetry related copies of each other. As an example, consider state 45 in Figure 1a,b. The density plot shows a localization or restriction of density to a band that loops the torus at $\psi_a = \psi_b$ which is clearly the organizing center. The phase plot shows it is a running wave

in the diagonal direction. The density is localized in the antidiagonal direction. There are no nodes in the transverse direction so the transverse oscillator quantum number is $n_t = 0$. The phase part of the diagram under the high-density region shows a phase advance of $8 \times 2\pi$ as the running wave loops the torus. The longitudinal quantum number is then $n_l = 8$ and the state is assigned $(n_t, n_l) = (0, 8)$.

A second example is state "25 + 26" in Figure 1 which has its density localized and organized about $\psi_m = 0$. The ψ_m direction is then the localization direction. In the phase diagram, the eigenfunction is again a running wave in the ψ_n direction, and because of the nodal line and the two maxima about it, it is a singly excited oscillator along ψ_m centered at $\psi_m = 0$. The phase advance counted in the ψ_n running wave direction over the loop is counted under one of the dense lines and gives the phase advance as $l = 2$, and the assignment is $(n_t, n_l) = (1, 2)$.

Generally, if m independent resonances are active in the reduced space of N dimensions, localization will appear in m directions, and the wave function will be of the running wave type in the remaining $N - m$ directions. The organizing center is then the Cartesian product of the $N - m$ independent loops around the torus. These loops guide the running waves, are orthogonal to the localized directions, and pass through the common center of each localized direction. The organizing structure is of dimension zero for $m = N$, that is, a point; for $m = N - 1$ it is a line; for $m = N - 2$, it is a plane, etc. The quantum numbers for the m directions transverse to the organizing center are obtained from node counting in each of the transverse directions. The quantum numbers in the organizing center are obtained from a phase count around each of the independent loops (lines in our diagrams) that make up the organizing center.

If $m = 0$, the whole reduced configuration space acts as an organizing center. The N quantum numbers are obtained by phase counting about any loop in each ψ_k direction, that is, for each ψ_k, any line in the diagram parallel to ψ_k. Since there are no restrictions in reduced space and since the cyclic angles run free, there are no restrictions in the original D dimensional space, and all motions are simply continuously distorted normal modes.

For $0 < m < N$, there are m restrictions in the reduced and also in the original displacement and configuration space. For assignment $N - m$, quantum numbers come from counting phase advances along the $N - m$ independent loops in the $N - m$ dimensional organization center and from m further quantum numbers obtained from node counting in each of the m independent transverse directions to the organizing structure. The K_k are F additional quantum numbers used to make the total needed of D. In the original space, the m restrictions mean that m original modes will be coupled and $D - m$ ones will be free.

6. First Example: DCO

At this point, an example can help. Figure 1a,b shows the $P = 8$ wave function density and phase plots for DCO. The original modes are the local albeit near normal DC stretch (m), CO stretch (n), and the bend (b). Since $\omega_m \approx \omega_n \approx 2\omega_b$, it is not surprising that the most important resonances in the Hamiltonian are (see Table 1) the two Fermi resonances based on $\omega_m \approx 2\omega_b$ and $\omega_n \approx 2\omega_b$ and the 1:1 and 2:2 stretch resonances based on $\omega_m - \omega_n \approx 0$ and $2\omega_m - 2\omega_n \approx 0$. Here, $P = n_m + n_n + n_b/2$, and we choose $P = 8$ with 45 states in it. Since $D = 3$ and $F = 1$ (the polyad), $N = 2$. Out of the four resonances, the Fermis turn out to define ψ_1 and ψ_2 as $\psi_m = \phi_m - 2\phi_b$ and $\psi_n = \phi_n - 2\phi_b$. Thereby, $d\psi_m/dt = d\phi_m/dt - 2d\phi_b/dt = \omega_m - 2\omega_b \approx 0$ and $d\psi_n/dt = \omega_n - 2\omega_b \approx 0$. These equations tell us that ψ_m will be fixed when the bend and the DC stretch are in resonance, and ψ_n is fixed when the CO stretch couples to the bend. Formally, we start with the four resonances

$$r^{(1)} = (1 \ -1 \ 0), \quad r^{(2)} = (2 \ -2 \ 0),$$
$$r^{(3)} = (1 \ 0 \ -2) \qquad r^{(4)} = (0 \ 1 \ -2) \quad (21)$$

From the matrix with the columns, $\vec{r}^{(j)}$, the rank, that is, the number of linearly independent vectors, is found to be two; therefore, $N = 2$. The two remaining columns after rank reduction are a basis for R space. The number of polyad constants of the motion is $F = 1$ as $D = F + N$. Any vector orthogonal to the R basis vectors will serve as S and $s_n = (1, 1, 1/2)$ suffices. Now, the classical polyad conserved quantity is

$$K = I_m + I_n + I_b/2 \qquad (22)$$

which is the same as the one used by the experimentalists[10] who noted a near $\omega_m{:}\omega_n{:}\omega_b = 2{:}2{:}1$ ratio of the fundamentals. With K determined, eq 11 allows us to define M as

$$M = \begin{pmatrix} 1 & 0 & 0 \\ 0 & 1 & 0 \\ 1 & 1 & 1/2 \end{pmatrix} \qquad (23)$$

and

$$G(I, \psi) = (\psi_1, \psi_2, \psi_3)M \, (I_1 \ I_2 \ I_3) =$$
$$\psi_1 J_1(I) + \psi_2 J_2(I) + \psi_3 K(I) \quad (24)$$

This equation says

$$J_1 = I_m \quad J_2 = I_n \qquad J_3 = K \qquad (25)$$

Using eq 14, we obtain

$$\phi_m = \partial G/\partial I_m = \psi_1 + \psi_3$$
$$\phi_n = \partial G/\partial I_n = \psi_2 + \psi_3$$
$$\phi_b = \partial G/\partial I_b = \psi_3/2 \qquad (26)$$

with inversion

$$\psi_m = \psi_1 = \phi_m - 2\phi_b$$
$$\psi_n = \psi_2 = \phi_n - 2\phi_b$$
$$\theta = \psi_3 = 2\phi_b \qquad (27)$$

which means that n_n and n_m appear in eq 17 since $n_j = p_j$.

Figure 1a,b exhibits the density and phase plots for the eigenfunctions converted from the n representation to the ψ_m, ψ_n space using eq 20. Before Figure 1 was constructed, the density and phase of each eigenstate were put on opposite sides of a single card. Then just on the basis of topology, the cards were sorted into the three obvious suites (ladders) that form the corners of the triangular arrangement of diagrams. The reader can even, without interpretation, note the gross similarity in the density and phase plots for the states in the corners. Some states first resisted sorting, and we return to them later. At this point, many strategies based on topology for placement of the cards are possible. We describe one here. On the basis of the unrestricted density, we conclude that there is normal mode motion. Since $N = 2$, there are two independent loops which can be taken along ψ_m and ψ_n. From the phases, the increasing in energy indexed states 1, 2, 4, 6, 7, and 10 were obvious to group into one row as they all have a zero phase advance in the n (i.e., CO) direction. State 1 starts with phase advance 8 in the m direction, and going along the sequence, the phase advance decreases by 1. Rows further down in the arrangement of the figures give similar sequences for higher values of phase advances in the n direction. Closer inspection shows that the $n_n = n_{CO}$ index changes upward in this sequence; that is, the CO stretch gains quanta as the DC stretch loses them. The CO stretch quantum number remains well-defined while the DC stretch is becoming less well-defined. The reason for this becomes clear by "flipping the cards" in the top row to see the density plots which show a state 1 to 10 evolution which has no localization, that is, no resonances up to state 7 implying a clear single configuration normal mode state for the "upper left" region with n_b obtained from the polyad relation. We call class A all of the states with well-defined values of n_m and n_n, that is, the normal mode states.

Starting with state 19 and moving left, a localization, that is, a resonance, is seen for 19, 15, 12, and perhaps 10. Here, on the average, $\psi_m = 0$ is for these states implying $d\psi_m/dt = d\phi_m/dt - 2d\phi_b/dt = \omega_m - 2\omega_b = 0$. Here, such "upper right" states are DC stretch−bend resonance states indexed by their nodes (vertical white strips) going left from 0, 1, 2, and 3, respectively. n_m and n_b no longer exist and are not good quantum numbers. Since ψ_n is not restricted, mode n is not locked with mode b nor with mode m either; that is, the stretch n is decoupled. The three good dynamic quantum numbers are P, the number of transverse nodes n_t, and $l = n_{DC} = n_n$ which is zero. State 10 is clearly transitional and lies in phase space on the border of

the region where normal mode dominates and that in which the Fermi resonance dominates. This Fermi group was called class B in ref 9. State 19 clearly lies in the middle of this region and 15, then 12 are further out. State 10 can be multiply assigned by either $n_{CO} = 0$, $n_{DC} = 3$, and $n_b = 10$ (normal mode) or $P = 8$, $n_l = n_{CO} = 0$ and $n_t = 3$ (Fermi resonance).

The left and right corners can now be built up from the shuffled, albeit energy ordered, deck by similar arguments. For the normal mode states as the row position goes down, n_{CO} increases progressively by one, and n_b decreases by two. For the Fermi states, again, n_{CO} increases down the rows giving states similar to the higher rows but with less excitation in the coupled modes DC stretch and bend. State 18 is clearly normal mode with $n_{CO} = 3$, $n_{DC} = 5$, etc. State 23 is transitional, the phase is pushing for a normal and the density is pushing for a Fermi classification. State 24 is Fermi with $n_l = 1$, l for longitudinal, from a phase count made along a high-density line. Since there are no nodes in 24's transverse localized direction, we assign an $n_t = 0$ as the quantum number that essentially describes the excitation of the deviation from exact locking. $(P, n_t, n_{CO} = n_l) = (8, 0, 1)$ is the assignment.

Dropping to the states, placed eventually in the lower right corner (class C) a common localized diagonal trend at $\psi_m = \psi_n$ in the density and phase advances, is noted for the bottom four rows with state 39 transitional with the Fermi resonance. Since $d\psi_m/dt = \omega_m$, $d\psi_n/dt = \omega_n$. Here, $\omega_{CO} = \omega_{DC}$, indicating that the 1:1 and 2:2 resonances are active. As the columns move left, the nodes increase. The phases decrease from 8 as the row increases supplying quantum numbers. The organizing structure is diagonally localized and is $\psi_m = \psi_n$. For example, state 45 has no nodes and can be given a transverse quantum number $n_t = 0$. In the nonlocalized rotating direction along the diagonal organizing structure, the phase diagram gives a longitudinal quantum number as the phase advance of $n_l = 8$. Therefore, an assignment $(P, n_t, n_l) = (8, 0, 8)$ can be made. Further insight can be gained by changing to diagonal ψ_+ and antidiagonal ψ_- coordinates as $\psi_+ = (\psi_m + \psi_n)/2$ and $\psi_- = (\psi_m - \psi_n)/2$. Now, state 45 loops as a rotor along ψ_+ at $\psi_- = 0$. The basis functions are $\exp[i(n_m\psi_m + n_n\psi_n)] \rightarrow \exp[i(n_m + n_n)\psi_+ + i(n_m - n_n)\psi_-]$. The factor associated with the uncoupled rotor along ψ_+, that is, $\exp[i(n_m + n_n)\psi_+]$, factors out of eq 20 leaving the total wave function localized about ψ_-. As $\psi_+ \rightarrow \psi_+ + 2\pi$, the rotor must advance phase by $2\pi(n_m + n_n)$ which then is n_l. As such, 8 quanta are tied up in mode n to mode m or DC to CO lock. n_m and n_n are no longer good quantum numbers but are replaced by n_l and n_t. Neither ψ_m nor ψ_n are separately localized, meaning n and m are not locked to b which implies that the bend is decoupled. Since now $P = n_m + n_n + n_b/2 \rightarrow n_l + n_b/2$, it is clear that $n_b = 0$ for $P = 8$.

Clearly, three ladders have been established. The CO stretch to bend Fermi resonance which appears prominently in the Hamiltonian and would give a horizontal organizing structure, that is, localization along ψ_n, is absent from this polyad. Table 2 gives the summary of the assignment. Table 2 and Figure 1 show for each state one or more of the symbols A (normal), B (Fermi), and C (m:n) to indicate the ladder the state is on. Transitional states are also given. The states in the middle of the diagram are more extended in density over the configuration space. In this sense, they are the tops of the ladders, and the corner states are at the bottom. From the point of view of energy, the ladder starting with state 45 is upside down. This is not strange if one remembers that all states in the polyad have the same total excitation. They vary only in the distribution of the excitation. The middle states exhibit both a classical and a

TABLE 2: Classification and Assignment of All States of Polyad 8 of DCO[a]

no.	energy	class	n_l	n_t	n_m	n_n	no.	energy	class	n_l	n_t	n_m	n_n
1	8931	A			8	0	23	13163	A			4	3
2	9845	A			7	0			(B)	3	4		3
3	10485	A			7	1	24	13184	B	1	0		1
4	10614	A			6	0	25	13233	B	3	3		3
5	11216	A			6	1			(C)	3	1		
6	11236	A			5	0	26	13256	B	2	1		2
7	11704	A			4	0			(C)	3	0		
		(B)	0	4		0	27	13379	B	3	2		3
8	11779	A			6	2	28	13488	B	2	0		2
9	11800	A			5	1	29	13527	B	4	3		4
10	12010	B	0	3		0			(C)	4	1		
		(A)			3	0	30	13569	B	3	1		1
11	12226	A			4	1	31	13579	A			4	4
		(B)	1	4		1	32	13689	B	4	2		4
12	12244	B	0	2		0			(C)	5	2		
		(A)			2	0	33	13752	B	3	0		3
13	12325	A			5	2	34	13785	C	5	1		
14	12471	B	1	3		1	35	13848	B	4	1		4
		(A)			3	1			(C)	5	0		
15	12521	B	0	1		0	36	13900	C	6	2		
		(A)			1	0	37	13985	C	6	1		
16	12656	B	1	2		1	38	14023	C	7	2		
		(A)			2	1	39	14055	C	8	3		
17	12712	A			4	2	40	14086	C	6	0		
		(B)	2	4		2	41	14130	C	8	2		
18	12812	A			5	3			(B)	5	1		5
19	12838	B	0	0		0	42	14211	C	7	1		
20	12884	B	2	3		2	43	14330	C	7	0		
21	12902	B	1	1		1	44	14383	C	8	1		
22	13031	B	2	2		2	45	14540	C	8	0		

[a] First column gives the number of the states ordered by increasing energy. The second column gives the value of the energy in cm^{-1}. The third column gives the class into which the state is put. Columns four and five give longitudinal and transversal quantum numbers n_l and n_t for states of classes B and C. Columns six and seven give quantum numbers n_m and n_n of the basic modes for states of class A. Because for states of class B the longitudinal motion runs into the n direction, the longitudinal quantum number can also be interpreted as the quantum number of this local mode and is repeated in the corresponding column. For many states, alternative classifications are possible. Therefore, we first give the most natural or obvious classification and second give in the line below the alternative classification, put in parentheses. For states 25, 26, 30, 31, 33, and 34, we have used the demixing described in the main text to decide the classification.
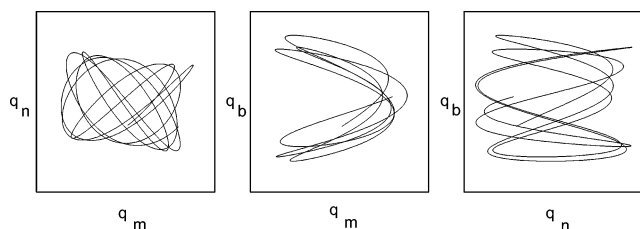
quantum mixing, a concept that we return to below and which enables us to pin down the dynamics in these states after some additional nonsystem specific discussion.

Since the organizing structure of a ladder of states should be orthogonal to the localized directions, m in number, in the states of the ladder, they should be subsets of dimension $N - m$ on the N dimensional torus. Hence, for DCO, N was 2. The upper right and the lower right states were states based on one active resonance. Hence, both had one-dimensional organizing structures, that is, lines. The former was the line perpendicular to the ψ_{DC} direction at $\psi_{DC} = 0$. The latter was the diagonal perpendicular to the resonance localization in the antidiagonal.

7. Lift and the Wave Function in Displacement Coordinates

To recover the dynamics in normal mode phase and configuration space, we must start with a trajectory in (J, ψ) space which represents the organizing structure. Since we are looking for a motion that when quantized gives the ladder of states, we start the procedure using the most localized state on the ladder (in DCO the states in the right-hand corners of Figure 1). These states lie at the center of the phase space resonance zone of the ladders coupled modes. Of course, the organizing structure helps

Extracting Dynamics from Spectroscopic Hamiltonians

J. Phys. Chem. A, Vol. 111, No. 16, 2007 **3055**

Figure 2. This figure shows the projection into the various 2-dimensional planes of displacement coordinates for the lifted trajectory belonging to quantum state 24 of polyad 8 for DCO. Part a shows the projection into the $m-n$ plane, part b shows the projection into the $m-b$ plane, and part c shows the projection into the $n-b$ plane respectively. The units are arbitrary.

us find this trajectory which will be transformed in reverse from what was done in section 4 to (I, ϕ) space and then on to (p, q) normal coordinates space using the harmonic model. To start this search, estimates of the actions will be useful. For uncoupled modes, the assigned n_j quantum numbers using $J_j = I_j = n_j + 1/2$ will suffice. To obtain estimates of the initial actions the quantum mechanical average of the J_j can be used and trivially computed from the known wave function as

$$\langle J_j \rangle = \left\langle \Psi \left| -i\frac{\partial}{\partial \psi_j} \right| \Psi \right\rangle = \sum_n |c_n|^2 n_j \qquad (28)$$

The initial ψ_j is obtained from any point on the organizing structure. With this, we now have the initial conditions to use in Hamiltons equations to get the above-discussed trajectory as $(J(t), \psi(t))$. Equations 10 and 14 allow the transformation back to $(I(t), \phi(t))$ with the caveat that the ψ used to describe the reduced configuration space are those obtained from eq 14.

With $(J(t), \psi(t))$, we construct the cyclic angles θ by integrating

$$\theta_j(t) = \theta_j(0) + \int_0^t ds \frac{\partial H}{\partial K_j}(J(s), \psi(s)) \qquad (29)$$

As discussed earlier for reasons given, we then assume some idealized harmonic model for the elementary degrees of freedom and form the displacement $q(t)$ and its conjugate momentum $p(t)$ as

$$q_j(t) = \sqrt{2I_j(t)}\cos(\phi_j(t)) \qquad p_j(t) = \sqrt{2I_j(t)}\sin(\phi_j(t)) \qquad (30)$$

Most often, the motion retains its gross topology when we simplify eq 30 by replacing $I_j(t)$ with $I_j = \langle I_j(t) \rangle$.

Let us again consider our example for DCO. Figure 2 shows the lifted trajectories for state 24 projected onto the coordinate planes. The most striking feature is the shallow U-shaped region or strip traversed by the trajectory in the q_m/q_b plane. This shape could be anticipated for the $m-b-b$ resonance where in one period of motion two sweeps in the m local mode must be made for one sweep of the mode b. The n motion being uncoupled to the m or b is typical of a free oscillator. In some loose sense, the plane of the U oscillates with frequency $\omega_{CO} = \omega_n$ along the CO bond direction.

Perhaps, more instructive is the ability to anticipate the wave function's three-dimensional (3D) topology in displacement coordinate space. Clearly, the factor in the amplitude of the wave function in 3D space in the q_n direction is that of an oscillator with the frequency ω_{CO} and $n_{CO} = n_n$ nodes. In planes perpendicular, a U-shaped density cut must exist with a total excitation of $P - n_n = P - n_{CO}$ quanta in units of the stretch frequency.

The nodal properties of the density on the U-shaped nodal region has n_t as the number of nodes, that is, U-shaped white strips. This is clear from the fact that a zero-valued point in the locked region must always transform to a zero-valued point in the lifted region. Since in the limit of weak coupling the U becomes very shallow and goes to a wave function approximating a product of the DC stretch and n_b bends it is clear that n_t can be associated with n_m and the number of nodes perpendicular to the U. Since $n_b = 2(P - n_{CO} - n_t)$, we expect 14 nodes perpendicular to the locus of the organizing U. State 24 is rather simple in appearance with low continuous deformation or mixing; a cut in 3D displacement space was made at a node of q_b, and the expected wave function could be seen. Other states range in appearance in 3D from "not so clear" to "not clear at all" so that such comparisons cannot be made.

Turning to state 45, it is worth noting that for this class of states the classical dynamics is completely chaotic in the sense that we cannot detect any low to moderate coupling region of reasonable size. The quantum mechanics is of course totally regular, and the lift appears in the q_n versus q_b plane (see Figure 4c,g in ref 9) as a trajectory circling and running back and forth along lines parallel to the long axis of an ellipse. The long axis slope basically tells us that the coupled $m-n$ mode bond oscillators are phase locked. If the slope is positive, then the modes move in a quasi-symmetric manner, increasing their extension and decreasing their extension together. The prefix "quasi" is used because DCO is a bent molecule. In a sense, this motion is analogous to a symmetric normal mode as opposed to the uncoupled local mode motion retained by the bend mode. If the slope is negative, then a quasi-antisymmetric "normal mode" motion occurs and so forth. Unfortunately, our theory cannot determine this slope which we would only know if we could insert and pin down the value of the relative phase (π is antisymmetric, 0 is symmetric). That in principle should appear in the arguments of the trigonometric functions in our correspondence in relation to eq 30. Our figures were shown with zero phases, as in eq 30, giving a positive slope. Actually, the negative one is correct. To clear this up, we sought a 3D periodic orbit or near periodic orbit in displacement space associated with this state to observe its orientation. Because this is the highest state in the polyad and because lower polyads have qualitatively the same type of states, we could work at lower total excitation P where finding such a trajectory would not be difficult. In this case, the search was made easy because in ref 36 such an orbit was located and found to have a negative slope.

By studying other states with higher n_t values, it was seen that, as n_t increases, the distance the trajectory moves from the major axis increases although on the average these fluctuations are zero.

Returning to state 45 with $n_l = 8$ quanta in the lock and considering $P = n_m + n_n + n_b/2 = 8 \rightarrow P = n_l + n_b/2 = 8 + n_b/2 = 8$, we find $n_b = 0$. As we move up the rows of Figure 1 from state 45, n_l decreases by 1, and n_b increases by 2. As we move left columnwise, n_t increases which means out of phase motion is stronger countering the inphase dominant tendency. This latter effect makes anticipation and investigation of projections of the 3D displacement space wave functions quite difficult.

In 3D problems, the lift often becomes less and less informative as no simple describable motion is possible. In this case, assignments and the rough features of the 3D motion associated with them can still be obtained. In such a case, we take solace in the fact that the reduced dynamics is a complete and even simpler description of the motion.

Let us end this section with some remarks on the implications of the existence of decoupled directions and of the corresponding longitudinal quantum numbers. Imagine a state which is restricted in m directions; that is, m linearly independent resonances are active. The corresponding organizing center in the reduced configuration space has dimension $N - m$. Then, we sort the D new angles ψ_k into three different groups. The ones with indices 1 up to m are the directions in the reduced configuration space and perpendicular to the organizing center; that is, they are the new angles restricted to the neighborhood of some specific value by coupling. Those with indices $m + 1$ up to N are the ones in the reduced configuration space and parallel to the organizing center. The ones with the indices $N + 1$ up to D are the cyclic angles. All ψ must be linear combinations of the original ϕ. Therefore, there must be a matrix $\mathbf{U}$ such that $\psi = \mathbf{U}\phi$. This $\mathbf{U}$ plays the role of $(M^{-1})^T$ in eq 15. The new J with indices 1 up to m do not have well-defined values in the eigenstate under study; they are strongly mixed and are replaced by the transversal quantum numbers. The ones with indices $m + 1$ up to N have well-defined values given by the longitudinal quantum numbers. The ones with the indices $N + 1$ up to D are the polyad type conserved quantities and also have well-defined values. The relation between I and J is given by $I = \mathbf{U}^T J$. Next, assume that the original degree of freedom number j is not involved in any of the m active resonances. This implies that the first m of the ψ_k cannot depend on ϕ_j. Accordingly, the matrix elements $\mathbf{U}_{k,j} = 0$ for $k = 1, ..., m$. However, this implies also that $I_j = \mathbf{U}_{k,j}J_k$ does not depend on such J_k which do not have a sharp and well-defined value; that is, it only depends on longitudinal quantum numbers and conserved quantities. Therefore, it also has a well-defined sharp value.

In total, we have shown for such quantum states, for which original degree of freedom number j is not involved in any active resonance, the action I_j has a sharp and well-defined value determined by longitudinal quantum numbers of the reduced system and by polyad conserved quantities only.

8. Mixing

Clearly, there are states in Figure 1 that are not of types A, B, or C. The first cause of ideal type breakdown is accidental degeneracy, usually among states of the same ladder and with nearby energies. States 25 and 26, 30 and 31, and 33 and 34 fit this category. Suspecting, because of these pairs close energies, that they are accidental degeneracies, new states that are symmetric and antisymmetric combinations of the pair are created and found to be degenerate in energy and to have wave functions that are of a recognizable distortion of one of the classes of states. Here, by simply taking the sum and the difference of the nearly degenerate wave functions, they can be assigned as given in Table 2. In the lower left corner of Figure 1, pictures of the demixed states are given.

Of course, as P and reduced dimension increase, the states within and between zones mix in a way that little information can be gained from any demixing process. This means that the states are dynamically unassignable. They correspond to a quantum manifestation of chaos.

There remain a few states which are more difficult to interpret from a wave function inspection; they are states 29, 32, 34 (also after demixing with 33), 36, and 37. They all lie in the transition region between class B and class C. The difficulty comes from the coexistence of the organizational elements for classes B and C. They have winding numbers (0,1) and (1,1) on the toroidal configuration space, respectively. As a consequence, an infinity of other periodic orbits having various winding numbers l_m and l_n on the configuration torus exist, where the ratio between l_m and l_n can be any rational number between 0 and 1. Some of them, like the ones with loop numbers $l_m = 1$, $l_n = 2$ and $l_m = 2$, $l_n = 3$, are sufficiently important to have influence on a few quantum states and to impose a corresponding winding ratio in the path following the density crest of such functions. In the spirit of higher order perturbation theory, these orbits can be thought of as being created by the corresponding multiple combinations of the interaction terms in the Hamiltonian. Correspondingly, some quantum states should show a mixture of features belonging to classes B and C. Now, we briefly describe possible classifications of these states:

State 29. It can be interpreted as a perturbed class B state with quantum numbers $n_l = 4$, $n_t = 3$, or as a class C state with $n_l = 4$, $n_t = 1$. At the same time, it shows a pattern of winding ratio 1:2 (slope) indicating that the motion upon which this state is quantized is a trajectory that loops once around about the organizing center B with winding numbers (0, 1) for each time it loops around the organizing center C with winding numbers (1, 1). This would give a net $l_n : l_m$ winding ratio of 1:2 and could have features of both the class B and the class C states.

The appearance of longer resonant organizing structures in combination with shorter ones as templates demonstrates the idea of overshadowing. Typically, as the interaction terms become more important, one first recognizes the basic (shortest, simplest, template) organizing structures and, with increasing effect of the coupling, also some combinational ones.

State 32. This state can be interpreted as a perturbed class B state with quantum numbers $n_l = 4$, $n_t = 2$ or a class C state with $n_l = 5$, $n_t = 2$.

State 34. Before demixing with state 33, this state shows a 1:2 winding ratio and can be interpreted as a perturbed state of class C with $n_l = 5$, $n_t = 1$. After demixing, because of accidental degeneracy, it can be considered a class B state with $n_l = 5$, $n_t = 2$ or better as a state with slope 1:3, indicating a 1:3 winding ratio that loops around the 0:1 center of class B twice for every loop around the 1:1 center of class C.

State 36. This state shows a 2:3 winding ratio in its density crest. It can be interpreted as a perturbed state of class C with $n_l = 6$, $n_t = 2$ or a motion that loops the center of class C twice for each loop along the center of class B.

State 37. This state is the perturbed state of class C with quantum numbers $n_l = 6$, $n_t = 1$.

For higher polyads, one can expect ladders of states built on organizing centers with winding ratios such as 1:3 and 2:3.

Also, a few other states with lower energy that we have already assigned to class B can alternatively be interpreted as highly perturbed states of class C. See the alternative assignments given in Table 2. In the classification and assignments of highly perturbed states, we have also taken into account the energy spacings in various ladders of states to determine whether they appear to fit those of the particular sequence.

This multiple assignment is the dynamic generalization and explanation of the fact[37] that in quantum mechanics significant weights, often greater than 50%, can be found on a single configuration for each of two different basis sets usually formed from oscillator functions along orthogonal coordinate systems, for example, normal or local. Clearly, the dynamical explanation is more powerful as wave functions, or more precisely packets, follow classical organizing structures rather than coordinates chosen for convenience. The same dynamic forces that confine organizing centers also confine the wave packets which, when Fourier decomposed, give similarly confined wave functions.

Extracting Dynamics from Spectroscopic Hamiltonians

J. Phys. Chem. A, Vol. 111, No. 16, 2007 **3057**

Several comments are in order. First, note that each class of states can be viewed as a ladder of states with some shared rungs. The ladders overlap in energy so that states of different dynamic type interleave.

Second, in the experiment and in theoretical calculations, no local mode narrow scattering resonance states exist. We obtain them because no continuum sink is in the spectroscopic Hamiltonian and no decay is possible. Polyad 8 is made completely of scattering resonances, so only class B and C and mixed states exist. The reason for this is that the local modes are decoupled modes, and therefore, the DC motion, which points to the exit channel leading to D + CO, has no restraint on its tendency "to head out the door'', which in turn means that no narrow scattering resonances of class A exist. The other states that are scattering resonances exist because the DCO motion is restrained by the resonant coupling in the spectroscopic Hamiltonian. It is not clear that anything can be said on the basis of the dynamics about the lifetime of states in class B as opposed to those in class C. The absence in our assignment of states with $n-b-b$ Fermi resonant coupling is no mystery. Simply put, no region of phase space that corresponds to $n-b-b$ that is big enough to accommodate the semiclassical volume of such states exists up to polyad 8.

9. Nature of Phase Space, KAM Theory

Clearly, the nature of phase space in any energy region is what classically underlies the ability to identify ladders. As such, it is worth discussing very briefly how phase space changes as perturbations become more important and how resonant zones which underlie the ladders appear.

Let us introduce an auxiliary strength parameter λ into the resonant interactions of the Hamiltonian such that the Hamiltonian reads

$$H = H_0 + \lambda W \tag{31}$$

and let us imagine that we change λ from 0 to 1. At exactly the value 0, the system is integrable and all actions are conserved quantities. Then, the phase space foliates into invariant D dimensional surfaces of constant action. The motion on each of them is either periodic or quasiperiodic depending on the ratio of the various effective frequencies

$$\omega_k^{eff} = \partial H_0 / \partial I_k \tag{32}$$

All these invariant surfaces project 1:1 onto the configuration torus T^D, and the projected motion in configuration space is periodic or quasiperiodic. We can apply semiclassical Einstein−Brillouin−Keller (EBK) quantization (see section 2.5 in ref 38) to the system, and the quantization conditions pick out the tori whose action values fulfill the semiclassical quantization condition of the Bohr Sommerfeld type.

Now imagine that λ is different from 0 but very small, and assume that W contains at least two independent resonance terms. Then, H is no longer integrable, and according to the Poincare Birkhoff theorem (see section 6.6 in ref 39) all former invariant surfaces of constant action with rational ratios of their effective frequencies break. Each one is replaced by a finite number of periodic orbits, half of them stable and half of them unstable. The unstable periodic orbits lie in small chaotic regions, the stable ones are the centers of secondary invariant torus structures around them. As long as λ is sufficiently small, all such chaos layers and secondary structures occupy a very small relative fraction of the phase space volume, and in the limit $\lambda \rightarrow 0$ this volume goes to 0 exponentially.

The Kolmogorov−Arnold−Moser theorem (see chapter 9 in ref 40) guarantees that most of the invariant tori of the $\lambda = 0$ case survive small perturbations of the system; they only suffer a small continuous deformation. We call such surviving invariant surfaces the primary structures or primary tori. The primary tori still project 1:1 onto the configuration space, and they carry quasiperiodic motion. To regions of phase space which are mainly occupied by primary tori, we can still apply the semiclassical EBK quantization method. It now picks out tori or maybe small layers where the action integrals along the fundamental cycles of the tori fulfill conditions of the Bohr Sommerfeld type.

Next, λ is advanced. This increase in coupling is mirrored in spectra as one moves from low to high excitation. Then, more primary tori are destroyed, many secondary structures grow larger, and the chaotic layers become thicker in general. Some secondary structures correspond to rational frequency ratios for each of which the Hamiltonian contains a corresponding resonance term. These are the secondary structures which have a good chance to grow very large and to dominate a large volume in the phase space. In the case that such secondary structures are rather stable and contain large secondary invariant tori, then we can also apply the EBK semiclassical quantization to them.

For large λ, there is also a good chance that some of the chaotic regions grow large (for the formation of chaos in classical Hamiltonian systems, see ref 41), they appear in regions where several independent resonance zones overlap.[42] Usually, chaotic regions are highly structured; they have organization centers which in many cases are unstable periodic orbits. The average flow follows such organization structures and in most cases is rather simple. Then, in the quantum wave functions, we expect to find sequences of states which follow these classical average trends. Most important, in general, we have energetic coexistence of various large scale structures as organized flows and primary and secondary tori. Inside the secondary regions, the dynamics is different, albeit simple, from the normal modes in the primary zone.

For the reader interested in a classical analysis parallel to the quantum one given here, we refer to ref 43 where the spectrum of a model of water using an effective multiresonant Hamiltonian has been analyzed. This classical analysis requires much more numerical effort than the quantum one. Alternate classical approaches to this same problem have been given[31−35] and have been partially successful in assigning the spectrum as given by the Baggot model Hamiltonian for water.

10. CHBrClF Example

Here, the Fourier transform IR spectrum that probes the motion of the H atom in the ground electronic state of the chiral molecule CHBrClF shall be analyzed using the methodology described previously.

The normal modes associated with the H atom are a CH stretch (s) mode and two bending modes (a and b). Roughly in a, H bends in an arc encompassing the HCF plane and b bends back and forth in the BrCCl plane. Exact details are given in ref 8 (Figure 3 and Tables 1 and 8 therein) with all fitted parameters that appear in the spectroscopic Hamiltonian. Key to the dynamics is that $\omega_s \approx 2\omega_a \approx 2\omega_b$. This suggests, as is found in ref 8, that beside the usual linear normal mode diagonal terms and Dunham anharmonic diagonal terms the spectroscopic Hamiltonian should have as couplings two 1:2 Fermi resonances as $s-a$ and $s-b$ as well as a mixed Fermi resonance where one stretch adjacent level transition causes one adjacent level

transition in mode *a* and one in mode *b*. Additionally, it can be anticipated and it turns out that a Darling Dennison bend−bend two phonon transfer term is found to be important.

The anharmonically corrected zero-point energy is given as

$$E_0 = (\omega_s + \omega_a + \omega_b)/2 + \\ (x_{ss} + x_{aa} + x_{bb} + x_{sa} + x_{sb} + x_{ab})/4 \quad (33)$$

The polyad operator

$$P = n_s + (n_a + n_b)/2 \quad (34)$$

commutes with the Hamiltonian and allows it to be diagonalized, polyad block by polyad block, to yield in each polyad eigenvalues and eigenvectors expanded in the number representation, the expansion coefficients being given by the transformation matrix.

The original quantum *H* in ref 8 is given in normal order. We first bring it into symmetric order before we apply eq 1 to construct the corresponding classical *H*. This reordering of the terms creates a shift of the linear frequencies as

$$\omega_s^{new} = \omega_s^{old} - x_{ss} - x_{sd}/2 - x_{sb}/2$$

$$\omega_a^{new} = \omega_a^{old} - x_{aa} - x_{sd}/2 - x_{ab}/2$$

$$\omega_b^{new} = \omega_b^{old} - x_{bb} - x_{sb}/2 - x_{ab}/2 \quad (35)$$

From now on, the frequencies in classical expressions will be these new shifted frequencies, where we drop the upper index for simplicity. From *H*, we get the classical Hamiltonian function

$$H = -E_0 + \omega_s I_s + \omega_a I_a + \omega_b I_b + x_{ss} I_s^2 + x_{aa} I_a^2 + x_{bb} I_b^2 + \\ x_{sa} I_s I_a + x_{sb} I_s I_b + x_{ab} I_a I_b + k_{saa}\sqrt{I_s} I_a 2 \cos(2\phi_a - \phi_s) + \\ k_{sbb}\sqrt{I_s} I_b 2 \cos(2\phi_b - \phi_s) + k_{sab}\sqrt{I_s I_a I_b} 2 \cos(\phi_a + \phi_b - \\ \phi_s) + \gamma I_a I_b 2 \cos(2\phi_a - 2\phi_b) \quad (36)$$

This is a three degrees of freedom system with three actions I_s, I_a, and I_b and three angles ϕ_s, ϕ_a, and ϕ_b. The effective frequencies are given by $d\phi_j/dt = \partial H/\partial I_j$. Their rational ratios signal which resonances are important to include in the fit. At the rational ratio, the corresponding resonance terms have their effects magnified and new dynamics appears by effects of frequency and phase locking.

The classical Hamiltonian has the conserved quantity

$$K = I_a/2 + I_b/2 + I_s \quad (37)$$

which will be used to reduce the system to two degrees of freedom. Its value coincides with the quantum polyad number *P* up to the classical zero point value which is 1.

To make the reduction explicit, we apply the canonical transformation:

$$I_s = K - J_a/2 - J_b/2 \qquad \phi_s = \theta$$

$$I_a = J_a \qquad \phi_a = \psi_a + \theta/2$$

$$I_b = J_b \qquad \phi_b = \psi_b + \theta/2 \quad (38)$$

The definition of ψ_a and ψ_b reflect as previously explained a scheme by which the wave function can be expected to localize about $\psi_{a/b}$ if the $s-a-a/s-b-b$ Fermi resonance is influential

in the dynamics in that part of reduced phase space where the state $\Psi(\psi_a, \psi_b; K)$ resides.

The Hamiltonian in new coordinates is

$$H = -E_0 + \omega_s(K - J_a/2 - J_b/2) + \omega_a J_a + \omega_b J_b + x_{ss}(K - \\ J_a/2 - J_b/2)^2 + x_{aa} J_a^2 + x_{bb} J_b^2 + x_{sa}(K - J_a/2 - J_b/2)J_a + \\ x_{sb}(K - J_a/2 - J_b/2)J_b + x_{ab} J_a J_b + \\ k_{saa}\sqrt{K - J_a/2 - J_b/2} I_a 2 \cos(2\psi_a) + \\ k_{sbb}\sqrt{K - J_a/2 - J_b/2} I_b 2 \cos(2\psi_b) + \\ k_{sab}\sqrt{(K - J_a/2 - J_b/2)I_a I_b} 2 \cos(\psi_a + \psi_b) + \\ \gamma I_a I_b 2 \cos(2\psi_a - 2\psi_b) \quad (39)$$

By H_0, we denote the angle independent part of this Hamiltonian. The new angle θ does not appear in *H*; therefore, the conjugate action *K* can be treated as a parameter, and we have an effective two degrees of freedom system. This allows us to handle each polyad separately as an independent system.

As explained in sections 3 and 5, the number state basis functions $|n_s, n_a, n_b\rangle$ are represented as the periodic plane waves

$$\exp[i(n_s\phi_s + n_a\phi_a + n_b\phi_b)] = \exp(iP\theta)\exp[i(n_a\psi_a + n_b\psi_b)] \quad (40)$$

on the configuration torus of the reduced system.

At this point it is instructive to anticipate how an eigenfunction density plot might appear if the state lies in a resonance zone dominated by a particular resonance. By the localization logic in the ψ_b against ψ_a plane, if the $s-a-a$ resonance dominates, $\omega_s = 2\omega_a$ implies $d\phi_s/dt = 2d\phi_a/dt$, and therefore $\phi_s = 2\phi_a + \alpha$, α being a constant. In new variables, this condition is $\psi_a = \alpha/2$. Hence, all underlying trajectories and the wave function density should be in a ribbon running along the ψ_b direction and localized about the organizing structure $\psi_a = \alpha/2$. Similarly, the $s-b-b$ resonance should give a ribbon rotated to run along an organizing structure at $\psi_b = \beta/2$, β being a constant.

The $s-a-b$ resonance has $\omega_s = \omega_a + \omega_b$ which implies $\phi_s = \phi_a + \phi_b + \alpha$ giving in new variables $\psi_a = -\psi_b + \alpha$. Hence, the ribbon should run along the antidiagonal of the ψ_b against ψ_a graph drawn with periodic boundary conditions. A state dominated by the Dennison−Darling resonance has $\omega_a = \omega_b$ or $d\phi_a/dt = d\phi_b/dt$ which implies $\phi_b = \phi_a + \alpha$. The ribbon should run along the diagonal. Of course, if two resonances are active in the zone, then the wave function should be localized at the intersection of the ribbons or show manifestations of chaos. In the first case, the organizing structure would be the central point of the common area, and there would be no phase advance under the density as traversing the density does not loop the torus. In these single ribbon cases, the number of nodes running parallel to the organizing structure should give us one transverse quantum number and the phase advance under the ribbon, the longitudinal one. In the case of a point center, the two nodal patterns perpendicular to each ribbons organizing structure will supply both quantum numbers, the polyad value being the third one. Of course, if no localization is apparent as before the original mode, normal or local, description is appropriate, and the phase advances along a fixed ψ_a and that along a fixed ψ_b supply the quantum numbers.

In reality, the picture will be more complicated because of the symmetries in *H* which include the following:

A: The original system is invariant under the translation

$$\phi_a \rightarrow \phi_a + 2\pi \quad (41)$$

Extracting Dynamics from Spectroscopic Hamiltonians

J. Phys. Chem. A, Vol. 111, No. 16, 2007 **3059**

This induces the invariance under the translation

$$\psi_a \rightarrow \psi_a + 2\pi \qquad (42)$$

of the reduced Hamiltonian in new variables.

B: The original system is invariant under the translation

$$\phi_b \rightarrow \phi_b + 2\pi \qquad (43)$$

This induces the invariance under the translation

$$\psi_b \rightarrow \psi_b + 2\pi \qquad (44)$$

in new variables.

C: The original system is invariant under the translation

$$\phi_s \rightarrow \phi_s + 2\pi \qquad (45)$$

This induces the invariance under the translation

$$(\psi_a, \psi_b) \rightarrow (\psi_a + \pi, \psi_b + \pi) \qquad (46)$$

of the reduced Hamiltonian in new variables. Structures related by such an operation are equivalent. Note that the symmetry C indicates that the new angles double cover the space of the old angles. Symmetry C means an identification of opposite points on the reduced configuration torus.

D: All angles only appear as linear homogeneous expressions in the arguments of cosine functions. Therefore, the Hamiltonian is invariant under a simultaneous inversion of the angles. In old variables, this symmetry is

$$(\phi_s, \phi_a, \phi_b) \rightarrow (-\phi_s, -\phi_a, -\phi_b) \qquad (47)$$

In new angles, it is

$$(\psi_a, \psi_b) \rightarrow (-\psi_a, -\psi_b) \qquad (48)$$

This implies that to any given solution in terms of the action/ angle variables $\psi_a(t)$, $\psi_b(t)$, $J_a(t)$, and $J_b(t)$ of Hamilton's equations also the curve $-\psi_a(-t)$, $-\psi_b(-t)$, $J_a(-t)$, and $J_b(-t)$ is a solution of the equations of motion, that is, symmetry D is time reversal. Therefore, most orbits come in symmetry related pairs. Common exceptions are such orbits which coincide exactly with their symmetry image.

As in ref 7, polyad 8 with 81 states is considered. At the low end of the polyad, the lowest four states and the sixth state are "ribbons" localized at $\psi_b = \pi/2$ and $3\pi/2$. See Figure 3 (and Figure 1f,g of ref 7) for an example corresponding to such a state. Symmetry C tells us that really only one ribbon exists in each states density and phase diagram. Clearly these class A states are effected by a Fermi resonance with bending mode b interacting with the stretch mode. Clearly a transverse quantum number n_t given by the number of nodes in the ψ_b direction exists and for state 4 we find $n_t = 0$. The phase diagrams shows that if the phase advance is counted as the number of "black" stripes crossed as one moves along the organizing structure, say $\psi_b = \pi/2$, the result is three, therefore $n_l = 3$. Since rotors correspond to free motion and mode a is free $n_l = n_a$, the number of quanta in the normal bend, albeit continuously distorted, mode a. These results are summarized in Table 3(Table 1 of ref 7) where this type of state is labeled class A.

The lift here could be carried out since the organizing structure is known but it is unnecessary as the $\omega_s{:}\omega_a = 2{:}1$ ratio assures us that the classical motion must have a U shape on the q_s versus q_b plane at constant q_a. In the other planes, q_s versus q_a and q_b versus q_a with fixed q_b or q_s, respectively,
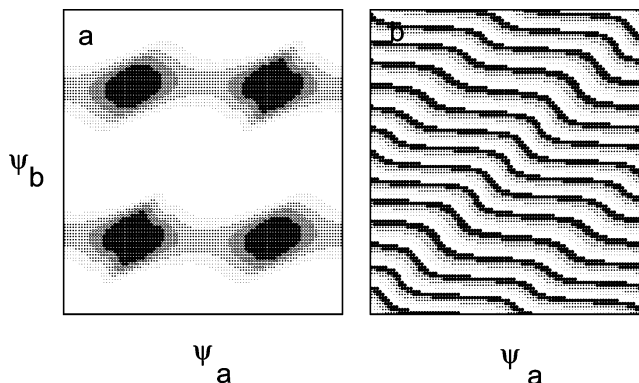
Figure 3. Semiclassical wave function for state 4 in polyad 8 of CHBrClF. Part a shows the density, and part b shows the phase. The horizontal coordinate ψ_a and the vertical coordinate ψ_b both range from $-\pi$ to π. In part a, darker gray means higher density. In part b, white means phase in the interval $[0, \pi/2)$, light gray means phase in the interval $[\pi/2, \pi)$, dark gray means phase in the interval $[\pi, 3\pi/2)$, and black means phase in the interval $[3\pi/2, 2\pi)$.

because of the decoupling of mode a, the motion must be quasiperiodic.

Information about the 3D wave functions can be obtained from these results. In the (q_s, q_b) plane, the density should localize on the U. Since a nodal point in the (ψ_a, ψ_b) space should transform to a nodal point in the U-shaped density, it is clear that the n_t transverse nodal "white" stripes should appear in the U-shaped density as white stripes. The U has $2P - n_a$ total quanta in units of ω_b. Also, since in the limit of weak coupling where the now shallow U would approach a normal mode picture on the (q_s, q_b) plane, we can adiabatically associate n_t with n_s and n_b with the nodes along the locus of the U. Since $2n_t$ replaces $2n_s$, $n_b = 2P - n_a - 2n_t$. With this, we expect 13 nodes perpendicular to the locus of the U. This offers an alternative equivalent assignment to $(P, n_t, n_l) = (P, n_t, n_a) = (8,0,3)$; that is, $(2P - 2n_t - n_a, n_t, n_l) = (2P - 2n_t - n_a, n_t, n_a) = (13, 0, 3)$.

The next ladder of states, class B, comes in as the energy rises, and energy is shifted to the faster modes. A typical state is state 7 in Table 3. Here, the density and phase diagrams are given in Figure 4. The density as shown at first looks quite like that of case A with $n_t = 1$ and $n_l = 1$. Closer inspection, with (ψ_a, ψ_b) cuts at different amplitude heights, shows a more diffuse nature than in class A which leads us to suspect that a continuously distorted (toward the Fermi resonance of class A) normal mode is involved. Since the normal mode is opted for, the phase diagram indicates $n_a = 1$ (moving along ψ_a) and $n_b = 13$ (moving along ψ_b) with n_s obtained from the polyad as 1. As such, class B is the normal mode and exists on primary tori.

At this point, the reader might object after noting that both class A and class B have quite similar phase diagrams that look rather like a normal mode and the density of B is rather like that of A. To ensure our values in this assignment, a trajectory was run starting at a high density point in the (ψ_a, ψ_b) plane of both types of states. For those states called A, the trajectory ran along the ribbon while for those called B it ran over all the plane often in the ψ_b direction. This confirms the assignment. B are distorted normal mode states which lie in regions of phase space containing primary tori but which are influenced by the nearby resonance zone containing the A states. From Table 3, it is seen that ladders A and B interleave. Also interleaving with B at higher energies are two ladders or classes of interlaced states called C and D. Still higher D dies out while a ladder E interleaves with C up to the top of the polyad.

TABLE 3: Classification and Assignment of All States of Polyad 8 of CHBrClF[a]

no.	energy	class	n_l	n_t	n_a	n_b
1	17451	A	0	0	0	
		(B)			0	16
2	17660	A	1	0	1	
		(B)			1	15
3	17863	A	2	0	2	
		(B)			2	14
4	18057	A	3	0	3	
		(B)			3	13
5	18147	B			0	14
6	18241	A	4	0	4	
		(B)			4	12
7	18349	B			1	13
8	18415	B			5	11
9	18542	B			2	12
10	18576	B			6	10
11	18720	D			7	9
12	18729	B			3	11
13	18779	B			0	12
14	18827	D			8	8
15	18898	B			4	10
16	18973	B			1	11
17	18994	C	8	3		
18	19010	C	8	3		
19	19058	D			5	9
20	19156	B			2	10
21	19195	D			6	8
22	19301	C	8	2		
23	19302	C	8	2		
24	19325	D			3	9
25	19340	C	7	3		
26	19345	B			0	10
27	19385	C	7	3		
28	19485	D			4	8
29	19533	D			1	9
30	19607	C	7	2		
31	19612	C	7	2		
32	19632	D			5	7
		(C)	6	3		
33	19681	C	8	1		
34	19681	C	8	1		
35	19704	D			2	8
36	19725	D			6	6
		(C)	6	3		
37	19837	D			0	8
38	19863	D			3	7
		(C)	5	3		
39	19891	C	6	2		
40	19900	C	6	2		
41	19952	C	7	1		
42	19953	C	7	1		
43	19991	D			4	6
		(C)	5	3		
44	20031	D			1	7
45	20122	C	8	0		
46	20122	C	8	0		
47	20129	C	5	2		
48	20159	C	5	2		
49	20185	D			2	6
50	20198	C	6	1		
51	20200	C	6	1		
52	20266	D			0	6
53	20327	D			3	5
		(C)	4	2		
54	20360	C	7	0		
55	20360	C	7	0		
56	20382	D			4	4
		(C)	4	2		
57	20413	C	5	1		
58	20417	C	5	1		
59	20468	D			1	5
60	20522	E	1	2		1
61	20574	C	6	0		
62	20574	C	6	0		
63	20592	C	4	1		
64	20596	C	4	1		
65	20667	E	0	2		0
66	20709	E	4	1		4
		(C)	3	1		
67	20750	E	3	1		3
		(C)	3	1		
68	20761	C	5	0		
69	20762	C	5	0		
70	20826	E	2	1		2
71	20908	E	1	1		1
72	20918	C	4	0		
73	20919	C	4	0		
74	21026	C	3	0		
75	21044	C	3	0		
		(E)	5	0		5
76	21054	E	0	1		0
77	21109	E	4	0		4
		(C)	2	0		
78	21172	E	3	0		3
		(C)	2	0		
79	21248	E	2	0		2
80	21339	E	1	0		1
81	21450	E	0	0		0

[a] First column gives the number of the states ordered by increasing energy. The second column gives the value of the energy in cm⁻¹. The third column gives the class into which the state is put. Columns four and five give longitudinal and transversal quantum numbers n_l and n_t for states of classes A, C, and E. Columns six and seven give quantum numbers n_a and n_b for states of classes B and D. Because for states of classes A and E the longitudinal motion runs in a coordinate direction, the longitudinal quantum number can also be interpreted as the corresponding quantum number in this coordinate direction and is then repeated in the corresponding column. For many states, alternative classifications in different classes are possible. Therefore, we first give the most natural or obvious classification and quantum numbers and second give in the line below the alternative class (in parentheses) the corresponding alternative quantum numbers. Note that in class C there are always two states with the same set of quantum numbers, which form a doublet pair. Quantum numbers n_t in column five are obtained by an oscillator node count; the other ones are obtained by phase count.
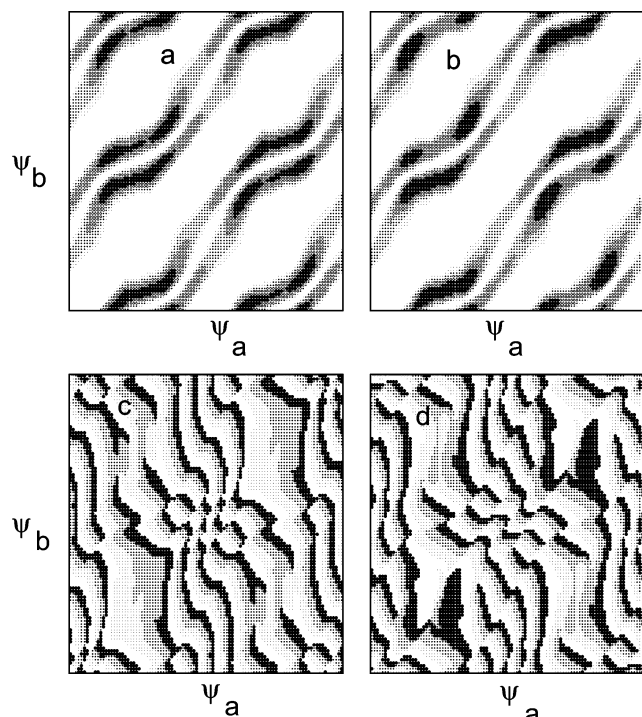
At this point, states E are easy to explain as they have densities again on a ribbon but this time oriented along ψ_b. For state 80, a typical E, density and phase are shown in Figure 5. Clearly, the s–a–a 2:1 = ω_s:ω_a Fermi resonance dominates
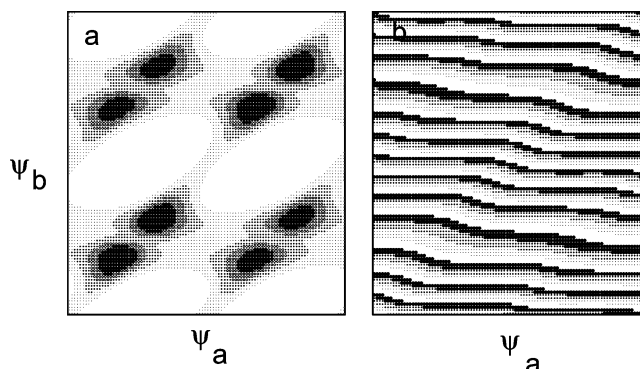
Figure 4. Semiclassical wave function for state 7 in polyad 8 of CHBrClF. Otherwise as Figure 3.
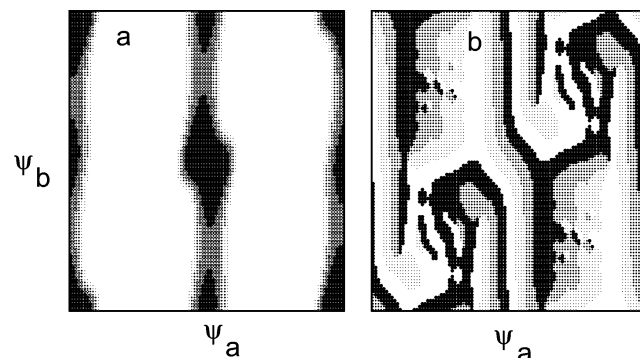
Figure 5. Semiclassical wave function for state 80 in polyad 8 of CHBrClF. Otherwise as Figure 3.

here, and $n_t = 0$ and $n_l = n_b = 1$ by parallel arguments to class A. Now, the lift of the organizing structure, the line $\psi_a = 0$, will give a U shape in the (q_s, q_a) plane. The assignment is $(P, n_t, n_l) = (P, n_t, n_b) = (8, 0, 1)$.

Now, let us come to class C that have "ladder rungs" that interleave with the B, D, and E ladders. These states are easily sorted in that the diagonal density pattern as typified by state 50 in Figure 6 appears indicating the influence of the DD, $\omega_a \approx \omega_b$ resonance. Here mode s is expected to be free as is indicated by the density ribbons that go around the torus. Modes a and b are locked. Notice in the density diagram that there seems to be two independent ribbons in each diagram. The $(\psi_a, \psi_b) \rightarrow (\psi + \pi, \psi_b + \pi)$ symmetry reflects each ribbon back onto itself and cannot account for the double ribbon. The ribbons have organizing structures at $\psi_b = \psi_a \pm \pi/2$. In the sorting and as seen in Table 3, these states appear in degenerate pairs, here state 50 and state 51 in Table 3. Both state 50 and state 51 have the same density, and the phase diagrams are qualitatively the same. However, the relative phase shift between the two ribbons is different. In states 50 and 51 for all ribbons, we find $n_t = 1$ and counting the longitudinal phase advance gives 12· 2π. However, considering that a factor of 2 comes from the doubling by symmetry D, we get $n_l = 6$ and quantum numbers $(P, n_t, n_l) = (8, 1, 6)$ can be assigned although a more meaningful assignment will be given below. The fact of the double ribbon and the pairing of states, here 50 and 51, point to the fact that what is occurring is that each ribbon corresponds to a single organizing structure state with the same energy. The interactions split the ribbons proportional to their overlapping density, this means more with increasing n_t. The higher the n_t, the more the single ribbon state is excited transversely and less localized perpendicular to the diagonal. As such, it overlaps the similarly broadened second ribbon more, and the splitting is larger, a feature which is seen in Table 3.

Extracting Dynamics from Spectroscopic Hamiltonians

J. Phys. Chem. A, Vol. 111, No. 16, 2007 **3061**

Figure 6. Semiclassical wave functions for states 50 and 51 in polyad 8 of CHBrClF. Part a shows the density of state 50, part b shows the density of state 51, part c shows the phase of state 50, and part d shows the phase of state 51. Otherwise as Figure 3.

The eigenfunction are linear combinations of the single ribbon states. The lift must be done for each ribbon individually. Consider the ribbon with the organizing structure $\psi_b = \psi_a + \pi/2$ which implies $\phi_b = \phi_a + \pi/2$ which means that the lift is given as

$$q_a = \sqrt{2I_a}\cos(\phi_a) \qquad q_b = \sqrt{2I_b}\cos(\phi_b) = -\sqrt{2I_b}\sin(\phi_a)$$

$$p_a = \sqrt{2I_a}\sin(\phi_a) \qquad p_b = \sqrt{2I_b}\sin(\phi_b) = \sqrt{2I_b}\cos(\phi_a)$$
(49)

The organizing structure in displacement coordinates (q_b, q_a) therefore is an ellipse. The corresponding trajectory moves counterclockwise. The ribbon with $\psi_b = \psi_a - \pi/2$, by similar logic, has an organizing structure that lifts to a trajectory representing elliptical motion in the clockwise direction. It is the quantization of these degenerate motions that gives rise to two near degenerate eigenstates which are the symmetric and antisymmetric linear combinations of the two rotational senses. The total atomic hydrogen motion can be viewed as hydrogen elliptically rotating in the (q_b, q_a) plane with angular frequency $\omega_a^{\text{eff}} = \omega_b^{\text{eff}}$ while at the same time it oscillates in the q_s direction at frequency ω_s^{eff}, the effective frequencies being those given as $\omega_k^{\text{eff}} = \partial H_0/\partial J_k$. The CH bond rotates with oscillating height on a cone.

To obtain n_s, it is instructive to note the following. If the ψ_b, ψ_a variables are changed to the diagonal $\psi_+ = (\psi_a + \psi_b)/2$ and $\psi_- = (\psi_a - \psi_b)/2$, then the free motion must be along ψ_+ and the localized oscillator motion must be along ψ_-. Each basis function then has the form

$$\exp[i(n_a\psi_a + n_b\psi_b)] \rightarrow$$
$$\exp[i(n_a + n_b)\psi_+]\exp[i(n_a - n_b)\psi_-] \quad (50)$$

The interaction mixes the basis function which retains a common "free" ψ_+ factor. Equation 20 then turns the ψ_- factor into an oscillator function $\chi_t^{\text{osc}}(\psi_-)$ with the resulting eigenfunction being free in ψ_+, that is, of the form $\exp[i(n_a + n_b)\psi_+]\chi_t^{\text{osc}}(\psi_-)$. This associates $(n_a + n_b)2\pi$ with the advancing phase, that is, $n_l \rightarrow n_a + n_b$. Therefore, $n_s = P - n_l = 2$ for states 50 and 51.

The "ideal" wave function in 3D is now obtained. We say "ideal" because in most cases the small perturbations left out of the effective Hamiltonian causing mixing between ribbons and the fact that we produce a cut at a fixed value of a third variable often makes obscure the true "ideal" shape based on dynamics. By the nodal conservation argument, we expect in the (q_b, q_a) plane a circular wave function with n_t nodes perpendicular to the circle. Since $P - n_s$ is n_l, we must have six quanta in the lock and therefore six nodes along the ellipse. In Table 3, an n_l value of 6 is given to reflect the idea.

The group of states called class D shows a mixture of features of class B and C allowing us to conclude that their phase space regions are close to each other. The phase functions like class B are still close to deformed periodic plane waves typical for normal modes, and the density functions show the beginning of localization about $\psi_b = \psi_a \pm \pi/2$ as in class C. As such, we can count the phase advances in the a and the b directions as we did in class B. Alternatively, we can count the phase advance along density crests in lines parallel to the diagonal and count nodes transverse to the structure as we did in class C. Accordingly, many states of class D have a double assignment in Table 3.

It is note worthy that the Fermi resonance $s-a-b$ seems to have no influence in this polyad. The lack of this term would allow an additional symmetry, namely, translation of either variable ψ_a or variable ψ_b by π. Our figures indicate that this symmetry is roughly but not exactly obeyed.

11. Bending Spectrum of Acetylene

Since in acetylene the trans normal mode (mode 4) and the cis normal mode (mode 5) that describe the low vibrations are both doubly degenerate, the effective Hamiltonian is expressed in terms of raising $a^\dagger$ and lowering a operators for the two-dimensional (2D) isotropic harmonic oscillator (see ref 44). These operators are labeled with d (right) and g (left) subscripts and are defined as

$$a_{\text{d}} = (a_x - ia_y)/\sqrt{2} \qquad a_{\text{g}} = (a_x + ia_y)/\sqrt{2} \quad (51)$$

where x and y represent the two equivalent rectilinear coordinates for the 2D oscillators. The d and g operators have the convenient property that the number operators corresponding to the conventional quantum labels for the 2D oscillators can be expressed as

$$v = v_{\text{d}} + v_{\text{g}} = a_{\text{d}}^\dagger a_{\text{d}} + a_{\text{g}}^\dagger a_{\text{g}} \qquad l = v_{\text{d}} - v_{\text{g}} = a_{\text{d}}^\dagger a_{\text{d}} - a_{\text{g}}^\dagger a_{\text{g}} \quad (52)$$

Note that on the basis of these definitions, both a_{d} and a_{g} destroy one quantum of vibration v (we replace n of the previous sections by v to make visual connection to the references 1 and 2 easier). As such, the four degrees of freedom quantum effective Hamiltonian $H(a^\dagger, a)$ (see ref 45 and eqs 1−4 in ref 2) is written in terms of the operators $a_{4\text{d}}^\dagger, a_{4\text{g}}^\dagger, a_{5\text{d}}^\dagger, a_{5\text{g}}^\dagger$ and $a_{4\text{d}}$, $a_{4\text{g}}, a_{5\text{d}}, a_{5\text{g}}$. This fitted Hamiltonian in the representation of the number states $|n\rangle = |v_{4\text{d}}, v_{4\text{g}}, v_{5\text{d}}, v_{5\text{g}}\rangle$ reproduces the energy of 82 spectrally inferred energy levels to ± 1.4 cm^{-1} up to 15 000

3062 *J. Phys. Chem. A, Vol. 111, No. 16, 2007*

Jung and Taylor

cm^{-1} where the top of the barrier to the isomerization of weakly bound (1000 cm^{-1}) vinylidene resides.

Conversion of $H(a^{\dagger}, a)$ using eq 1 gives $H(I, \phi)$. Besides the usual harmonic oscillator and Dunham anharmonic diagonal terms, there are four resonances all active when the ω_j of all four normal modes are close in value. The first resonance is a Dennison-Darling (DD) I type corresponding to vibrational energy transfer of two phonons between cis and trans modes at constant l_4 and l_5. The second resonance is a bending angular momentum transfer between cis and trans, and the third resonance is a DDII exchange of vibration and angular momentum between the two modes.

Associated with $H(I, \phi)$ are two conserved (polyad) quantum numbers, N_b, the total number of quanta of bend excitation, and L, the total vibrational angular momentum. They can be expressed as conserved actions as

$$K_a = (I_{4d} + I_{4g} + I_{5d} + I_{5g})/4 = (N_b + 2)/4 \quad (53)$$

and

$$K_b = (I_{4d} - I_{4g} + I_{5d} - I_{5g})/4 = L/4 \quad (54)$$

where the relation $n \rightarrow I + 1/2$ has been used so that K_a and K_b include the classical zero points.

With this $D = 4$, $F = 2$, and $N = 2$. The canonical transformation to reduced variables gives

$$\psi_a = \phi_{4d} + \phi_{4g} - \phi_{5d} - \phi_{5g}, \quad J_a = (I_{4d} + I_{4g} - I_{5d} - I_{5g})/4$$

$$\psi_b = -\phi_{4d} + \phi_{4g} + \phi_{5d} - \phi_{5g},$$
$$J_b = (-I_{4d} + I_{4g} + I_{5d} - I_{5g})/4$$

$$\theta_a = \phi_{4d} + \phi_{4g} + \phi_{5d} + \phi_{5g}, \quad K_a = (I_{4d} + I_{4g} + I_{5d} + I_{5g})/4$$

$$\theta_b = \phi_{4d} - \phi_{4g} + \phi_{5d} - \phi_{5g},$$
$$K_b = (I_{4d} - I_{4g} + I_{5d} - I_{5g})/4 \quad (55)$$

This transformation gives simple arguments of the cosine terms in the resonances of the reduced Hamiltonian which is now written

$$H(J_a, J_b, \psi_a, \psi_b; K_a, K_b) = 2\omega_4(K_a + J_a) + 2\omega_5(K_a - J_a) +$$
$$4x_{44}(K_a + J_a)^2 + 4x_{45}(K_a + J_a)(K_a - J_a) + 4x_{55}(K_a - $$
$$J_a)^2 + 8y_{444}(K_a + J_a)^3 + 8y_{445}(K_a + J_a)^2(K_a - J_a) +$$
$$8y_{455}(K_a + J_a)(K_a - J_a)^2 + 8y_{555}(K_a - J_a)^3 + 4g_{44}(K_b - $$
$$J_b)^2 + 4g_{45}(K_b - J_b)(K_b + J_b) + 4g_{55}(K_b + J_b)^2 +$$
$$2s_{45}[(K_a^2 - K_b^2)^2 + (J_a^2 - J_b^2)^2 - 2(K_a^2 + K_b^2)(J_a^2 + $$
$$J_b^2) - 8K_aK_bJ_aJ_b]^{1/2}\cos(\psi_a) + 2[r_{045} + r_{445}(2(K_a + J_a) - $$
$$1) + r_{545}(2(K_a - J_a) - 1)][(K_a^2 - K_b^2)^2 + (J_a^2 - J_b^2)^2 - $$
$$2(K_a^2 + K_b^2)(J_a^2 + J_b^2) - 8K_aK_bJ_aJ_b]^{1/2}\cos(\psi_b) +$$
$$1/2[r_{045} + 2g_{45} + r_{445}(2(K_a + J_a) - 1) + r_{545}(2(K_a - J_a) - $$
$$1)][((K_a + K_b)^2 - (J_a - J_b)^2)\cos(\psi_a - \psi_b) +$$
$$((K_a - K_b)^2 - (J_a + J_b)^2)\cos(\psi_a + \psi_b)] \quad (56)$$

K_a replaces N_b which is an approximate for the molecule itself but holds on the time scale of a few picoseconds.[6] K_b replaces L. Specifically, $4K_a$ is the total excitation of all elementary oscillators, including the zero point excitations. Since in the harmonic limit each of the four oscillators has, due to

zero point energy, an action equal to 1/2, the correspondence between the classical and the quantum mechanical conserved total action can be established as $N_b = 4K_a - 2$. K_b is one-fourth of the total vibrational angular momentum, $L = 4K_b$.
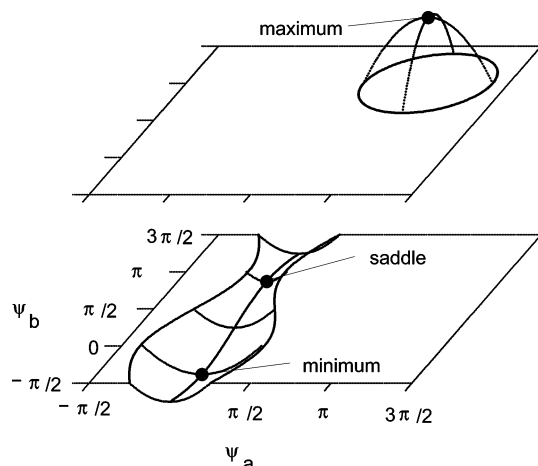
In our analysis, we shall limit ourselves to the polyad $L = 0$ and $N_b = 22$ setting aside the barrier. Previous efforts at an analysis using the Dunham expansion failed to explain the spectra, and theoretical studies have appeared which have analyzed various models of acetylene bending dynamics using quantum, semiclassical, classical, or all three mechanics[26,30,22,45] Each of these studies concluded that the dynamics was quite complicated at and above 10 000 cm^{-1} of bend excitation.

The initial steps of our analysis are similar to those of ref 30. There, a reduced dimension plot of an acetylene eigenfunction was exhibited. Unfortunately, the analysis did not continue. If it had, then there might be some differences from this work as the Hamiltonian used was somewhat different.

The work of ref 22 showed that a zero-order local mode basis set representing two noninteracting 2D harmonic oscillators expressed in terms of the local coordinates of the 2D oscillators could be used to assign 65 out of 144 states in the polyad 22. The assignment was done in the sense of ref 37 which said that if the overlap of an eigenfunction with an assignable, separable, zero-order model was greater than 50%, then the zero-order quantum numbers could be used to label the eigenstate. This was true because it was proven in ref 37 that if this were so the eigenstates could be derived from perturbation theory starting from the particular zero-order state. By this criterion, the 65 states could be assigned if the zero-order states were the ones of two 2D harmonic oscillators in a local mode representation. The low energy states had large projections onto a zero-order state which showed one hydrogen at equilibrium and the other oscillating. These type states heavily populate the lower end of the polyad though some existed higher up. Convergent overlap was also found for some eigenstates at the top of the polyad using zero-order states which had factors representing two hydrogens equally locally excited and rotating in a plane perpendicular to the carbon–carbon bond axis with a maximally allowed but oppositely sensed angular momentum. These states were called counter rotors (CRs). The analysis had three problems. First, 79 states, many in the middle of the polyad, could not be assigned. Second, the assignment was not unique in that the highest CR states also had greater than 50% weight, albeit less than in the local case, on the two 2D oscillator normal mode noninteracting basis. More seriously, these zero-order functions were not always tied to the dynamics, that is, to what we call the approximate but unique periodic orbits, planes, etc. about which the states and its nodes are organized. These problems were mostly resolved in ref 1 and ref 2 and here are completely resolved without the laborious periodic orbit and phase space searches of those papers.

We show that this "unassignable" spectrum can, without any but the most trivial calculation, be assigned and interpreted. The complexity is due, as always, to interleaving and sharing of several (here three) ladders or classes of states, which because of anharmonicity have nonuniformly spaced rungs. Here, the rungs of the ladders are assigned, and the dynamics upon which the rungs are quantized are revealed as follows.

At this point, the density and phase plots of the eigenfunctions need be drawn in the periodic (ψ_a, ψ_b) plane. The $-\pi/2$ to $3\pi/2$ variable range was most optimally revealing for density features, less repeats and less bisected structures in the plots. We

Extracting Dynamics from Spectroscopic Hamiltonians

J. Phys. Chem. A, Vol. 111, No. 16, 2007 **3063**

Figure 7. Illustration of the accessible energy range over each point of the two-dimensional configuration space for polyad $N_b = 22$, $L = 0$ of acetylene. The bottom and the ceiling of this slab are shown and act as effective potentials V_- and $-V_+$ respectively.

discovered by sorting plots with various angular ranges that three classes were important and also sufficient to assign the whole polyad.

In a local mode picture, all four degrees of freedom are degenerate, and in the normal mode picture used to construct the Hamiltonian, the effective frequencies are close. In addition, the faster normal mode has negative anharmonicity, whereas the slower normal mode has positive anharmonicity. Then, any excitation brings the effective normal-mode frequencies closer together. Therefore, over the whole polyad 22, all resonances are expected to be active. Hence, the number of independent active resonances is two, that is, $m = 2$. In the 2D reduced configuration space, this means that only point centers are important. In various groups of states, only the numerical values at which the angles ψ_a and ψ_b are locked change. Considering the negative values of the most important strength constants in the Hamiltonian (see Table 1), it becomes clear that at the lower end of the polyad the coupling must be at $(0, 0)$ in order to get positive values of the cosine functions and thereby negative values of the whole interaction terms. In the same way at the upper end of the polyad the angles must be locked around (π, π) in order to get negative values of the cosine functions and positive values of the whole interaction terms.

In order to understand this classification and their organization points well, it is useful to construct a corresponding equivalent potential picture as follows. For each value of the variables ψ_a and ψ_b, that is, for each point of the configuration torus, we determine the energy interval $[E_-(\psi_a, \psi_b), E_+(\psi_a, \psi_b)]$ for which this point is accessible to the classical trajectories within the specific polyad. This is done by varying the actions J_a, J_b over all their values that keep the elementary actions I_k (see eq 55) positive. The conditions are

$$|J_a| \leq K_a \qquad |J_b| \leq K_a$$

$$|J_a + J_b| \leq K_a - K_b \qquad |J_a - J_b| \leq K_a + K_b$$

Then for low energy in the polyad, the dynamics is very similar to the one in the potential $V_-(\psi_a, \psi_b) = E_-(\psi_a, \psi_b)$, and for high energies, it is very similar to the one in the potential $V_+(\psi_a, \psi_b) = -E_+(\psi_a, \psi_b)$.

The potential V_- shown schematically in Figure 7 has an absolute minimum point about $(0, 0)$ and extends uphill into a valley as shown. A saddle exists in the potential at $(0, \pi)$, ψ_b

being downhill and ψ_a being uphill. In the ψ_a direction, V_- opens onto a very flat plateau reached only at an energy above the saddle point. In $E_+ = -V_+$ there is a dome around an absolute maximum at (π, π). The potential wells at the centers $(0, 0)$ and (π, π) clearly indicate that they will support states that can be modeled as 2D anharmonic oscillators. Center $(0, \pi)$ should be based on a pendulum model in the ψ_b direction and an anharmonic oscillator in the ψ_a direction.

We draw this last conclusion from the fact that, classically, the ψ_b motion on the loop of the torus at $\psi_a = 0$ runs along the minimum of the V_- in the ψ_a direction and can be viewed as a pendulum of length equal to the radius of the torus loop at $\psi_a = 0$. The pendulum is anchored at the middle of the loop. The stable fixed point is at $(0, 0)$, and the unstable one is at $(0, \pi)$, that is, at the saddle. Below the saddle, the model tells that the motion would be librational about $(0, 0)$. Above the saddle along ψ_b at $\psi_a = 0$, one would expect, classically, two counter rotatory motions that slow down as they pass the barrier (saddle) at $(0, \pi)$ and speed up over $(0, 0)$.

Anticipating that quantum densities will greatly aid sorting, quantum mechanics should show in the well at $(0, 0)$ states with 2D anharmonic oscillator state behavior in the two directions, ψ_a and ψ_b. As the energy increased, the ψ_b direction would evolve to a density similar to the librator of the pendulum, with density high for large swings and small for small swings. When tunneling through, the saddle is possible, and above, the ψ_a direction will remain an anharmonic oscillator until the plateau in the ψ_a direction opens up allowing the density to seek larger ψ_a values. The ψ_b loop direction will show, at energies around the saddle, pendulum-like standing wave states, which we will describe below. Near (π, π) in the dome potential, again, 2D anharmonic functions centered about (π, π) should appear with excitation inverse to energy. There should also be transitional states for energies at which the wells open up and widen, that is, states that have, in the various corners of our individual state diagrams, densities which look like sums of densities of states quantized about two or even three corners. If such a state is closer to a particular corner, the part of the density plot near that center is darker and more relevant for classification. Also, it is well to remember that because we are on a torus, outer lobes of wave functions centered on one center can do double duty and serve as lobes of a state at another center.

Obviously, the strategy of our assignment here will be to sort the 144 states first into energy ordered symmetry representations g^-, g^+, u^- and u^+ (g^- is used for most further explanations) and then by working symmetry by symmetry to further sort the states at each symmetry into three classes based on how well the density of the states seems to be positioned and seems to resemble what is expected of a state in the potentials organized about each of the three organizing points. Some states will fall uniquely into one class in that its density makes no sense other than as a state supported by the model of a particular organizing point and therefore will be able to be assigned using the quantum numbers of the centers model. Other states will have density over two or even three organizing points and will be able to be interpreted as organized and assigned by two or three models simultaneously, although usually a preference is shown for one of the three models.

Figure 8 shows the densities of the g^- states. They have been laid out in a triangular array in analogy to the potentials local extrema. As such closeness to $(0, 0)$ quantization appears at the lowest corner; to $(0, \pi)$ at the right angle (upper left corner) and to (π, π) at the right most corner. We call this table CB organized because it makes an assignment (the quantum
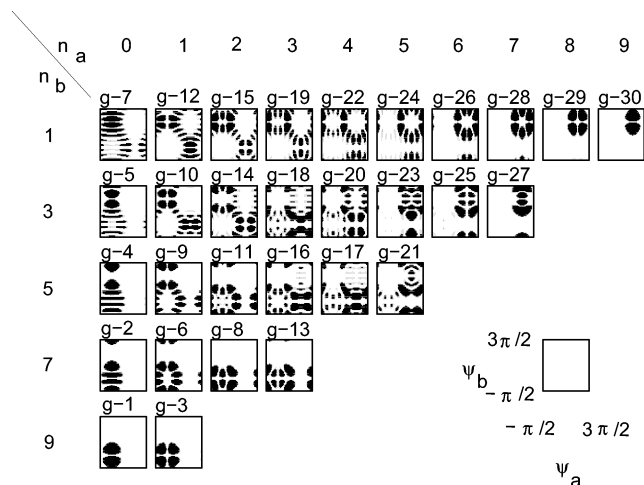
Figure 8. Density of all acetylene states of polyad $N_b = 22$, $L = 0$ belonging to symmetry representation g^- arranged according to classification scheme CB (compare part b of Figure 9). The horizontal coordinate is ψ_a going from $-\pi/2$ to $3\pi/2$, and the vertical coordinate is ψ_b also going from $-\pi/2$ to $3\pi/2$ exactly as in Figure 7. The coordinates and their range are also explained in the additional little frame in the lower right part of the figure. The columns and rows of the arrangement are labeled by the quantum numbers n_a^{CB} and n_b^{CB} respectively.
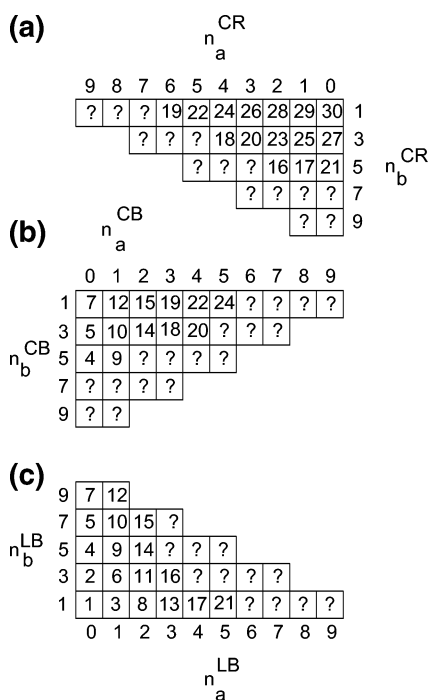
Figure 9. Arrangement of all acetylene states of polyad $N_b = 22$, $L = 0$ of symmetry representation g^- according to the classification schemes CR (part a top), CB (part b middle), and LB (part c bottom). If there is a state well described by the quantum numbers belonging to a box, then the corresponding state number is placed into the box. If not, then a question mark is placed into the box. The columns and the rows of each scheme are labeled by the quantum numbers n_a and n_b belonging to this scheme. Note that $n_b^{CR} = n_b^{CB}$ and $n_a^{CB} = n_a^{LB}$.

numbers n_a^{CB} and n_b^{CB}) based on referencing all states to the $(0, \pi)$ point. The label CB is used because we knew as will be explained later that $(0, \pi)$ would lift to a cross bend motion. Similar diagrams for the other corners (glance at Figure 9) will refer to the other corners and use the labels LB for local bender and CR for counter rotor. Once we discuss the expected

appearance of the above saddle pendulum states, the placement of the density diagrams becomes obvious in all of these arrangements; the states either look like the expected $(0, 0)$, $(0, \pi)$, or (π, π) density pictures or look as if they were in transition between two of the centers.

Several points about Figure 8 have not been explained yet. The first is how the n_a^{CB} and n_b^{CB} quantum numbers were assigned to states located far from $(0, \pi)$, and the second is what is the apparent localization about $(\pi, 0)$ seen in, for example, the g^-14 state. This latter point is easily answered. Simply, note that the point $(\pi, 0)$ was not used as an organizing point; the plateau was too flat there. All densities near $(\pi, 0)$, like the four dense peaks near $(\pi, 0)$ which seem to be an $n_a = 1$, $n_b = 1$ state based at $(\pi, 0)$, are outer lobes of LB, CR, or both oscillators that wrap around the torus from $(0, 0)$ and (π, π), respectively, at energies slightly above the V_- and V_+ plateau and have an enhanced density there because of their slow velocity. No class of such states exists; no $(n_a = 0, n_b = 0)$ state and no quantum numbers with n_a or n_b greater than or equal to two exist. For some symmetries at $(\pi, 0)$, there are too many states with an apparent assignment of 1,1 or 0,1 or 1,0 for them to be real states.

Holding the question of the n_a^{CB}, n_b^{CB} assignments off for the moment, let us now turn to the question of the appearance of the above barrier pendulum states before explaining the assignments of all g^- states. The point $(0, \pi)$ being a saddle implies by the pendulum model that above the saddle energy (or below that if tunneling occurs) there exist pairs of oppositely running rotating waves on the ψ_b loop at $\psi_a = 0$ which interfere constructively to give two kinds of standing wave states existing about the torus. Both standing wave states are amplitude modulated with the biggest peaks near to $(0, \pi)$ and the smallest near $(0, 0)$ which is why an oscillator model in ψ_b about $(0, \pi)$ would be incorrect. These states appear to be imposed on a nodal pattern which is $\sin(l\psi_b)$ for g^- and u^+ states and $\cos(l\psi_b)$ for g^+ and u^- states. Here, l is the total number of nodes seen in our diagrams when the torus is looped in ψ_b for $\psi_a = 0$.

To test that the tunneling and above saddle g^- states in the upper left corner of Figure 8 do indeed consist of two counter running waves, we have constructed such waves and confirmed that their phase advance was $2\pi l$ over the doubly transversed loop of length 4π. Since running waves are not of pure g^-, g^+, u^- or u^+ symmetry, for each state in the upper left corner of Figure 8, a matching $(0, \pi)$ organized state with similar energy and the same n_a^{CB} quantum number but of different symmetry representation was sought in symmetry class g^+. These restrictions made the choice obvious. The two states were then combined as $\cos(l\psi_b) \pm i \sin(l\psi_b)$, and the phase of the now rotating result was plotted on a 0 to 4π interval as required by our choice of the canonical transformation. The phase advance was counted as in our previous molecular examples, that is, over a high-density path in ψ_b and found to be $2\pi l$ in each case corresponding to the total number of nodes following the curves of high density. Hence, l is now established as the ψ_b indexing quantum number.

Hence, we place near $(0, \pi)$ states with oscillator behavior in the ψ_a direction and with high densities above and about $\psi_b = \pi$ near $\psi_a = 0$. We count nodes for n_a and l in the ψ_a and ψ_b directions, respectively.

For our diagrammatic purposes, l is inconvenient as its value changes with n_a^{CB} forbidding the use of l as a row index. For this reason, we introduce a quantum number n_b^{CB} uniquely determined by l, n_a^{CB}, and the symmetry representation which

correlates with the rows. For the four symmetry classes, it is given by

$$g^+: \quad n_b^{CB} = 10 - 2[n_a^{CB}/2] - l$$

$$g^-: \quad n_b^{CB} = 11 - 2[n_a^{CB}/2] - l$$

$$u^+: \quad n_b^{CB} = 12 - 2[(n_a^{CB}+1)/2] - l$$

$$u^-: \quad n_b^{CB} = 11 - 2[(n_a^{CB}+1)/2] - l$$

Here, [...] means the integer part of the number obtained from the fraction. The CB superscript is the class index for states localized about $(0, \pi)$, the choice of which along with LB for $(0, 0)$ and CR for (π, π) will become clear when the lift is discussed.

The pendulum model has now justified placing states from Figure 8 which are clearly organized about $(0, \pi)$ in the assignment tableau in Figure 9b. Figure 9b is CB organized and indicates the specific assignment for a given energy indexed state. In analogy to the triangle of points $(0, 0)$, $(0, \pi)$, and (π, π) in the density plots, the right angle was placed upper left, and the associated quantum numbers n_a^{CB} and n_b^{CB} index the rows and columns, respectively. Note that n_b^{CB} runs inverse and n_a^{CB} runs directly with energy. The symmetry g^- requires n_b^{CB} to be odd. The CB states organized about $(0, \pi)$ have now been assigned.

Next, an LB and a CR tableau, Figure 9c and Figure 9a, respectively, associated with the centers $(0, 0)$ and (π, π), respectively, were constructed. (n_a^{LB}, n_b^{LB}) and (n_a^{CR}, n_b^{CR}) must increase and decrease, respectively, with energy as they are respectively in or about a normal and inverted well at the bottom and the top of the polyad. Again, picture placement is easy but assignment far from the naming corner is often undoable, and any box noted as such is filled with a question mark. Multiple assignments are seen in the tableau and in Table 4 which records all of the assignments. For example, in g⁻14, note that LB and CB assignments have been made; g⁻20 has CR and CB assignments. Simply put, a state like g⁻20 has significant density in two places, and the system will have high probability of being organized about (π, π) and $(0, \pi)$, respectively, where it acts as an excited CR and an excited CB state, respectively. The best assignments are the ones on which a state density diagram is closest to the corners of the respective tableau.

A simple scheme gives a formal assignment of all states according to each class if one does the following procedure. In tableau LB (Figure 9c), move all columns up to the $n_b^{LB} = 9$ line. A CB tableau shape is achieved which is superimposed on the CB shape in Figure 9b. Erase the question mark in any box, and replace the question mark with a number. Now, shift the rows in Figure 9b right to $n_a^{CB} = 9$, superimpose with the CR tableau of Figure 9a, and erase as before. Now, reverse the procedure starting with the CR rows moving left to CB and then the CB columns moving down to $n_b^{CB} = 9$, superimpose, and erase. No more question marks exist, and formal and physically based assignments are achieved in the g^- symmetry sector. The Figure 8 assignment is now clear. Again, multiple assignments are seen, and the best assignment is the one closer to the corners. Note that we have now justified all quantum numbers in all schemes but only those included in Table 4 are deemed meaningful.

The transition regions deserve a bit more clarification. Figure 8 clearly shows the smooth transition in nodes but not in amplitude between the classes. Consider moving from CR to CB along the top row and viewing all of the states from the (π, π) point of view; n_a^{CR} then goes up by 1 at each step if smaller peaks are counted. Similarly up along the first column, the oscillator assignment was noted for LB to CB in the CB scheme. Going down below the saddle, CB pendulum states are librators converting to oscillators as the pendulum model anticipates connecting CB to LB. State g⁻21 clearly looks like a state in which CR is fading and LB is emerging; g^- does not have enough states to track this better. It is not surprising that if a lift is carried out along the density rich antidiagonal line, that the axis switching motion of reference 1 is obtained. In ref 2, the CB classification was not used. The CB corner was treated as excited LB along ψ_b and excited CR along ψ_a. We have discussed why the CB view presented here is favored.

At this point, the assignment story is complete, and the method can be used for other symmetry representations with equal success. At the end, all states with their assignments are given in Table 4 which is energy ordered. A short excursion to justify the symmetry ideas follows. The two basic symmetries are parity σ_v and g/u symmetry i as

$$\sigma_v(\psi_a, \psi_b) = (\psi_a, -\psi_b) \tag{57}$$

$$i(\psi_a, \psi_b) = (\psi_a, \psi_b + 2\pi) \tag{58}$$

These symmetry properties can be used to explain the appearance of symmetry doublets among the eigenfunctions that would be evident from the plots in Figure 8 and its other symmetry analogues. They would have pairs of states of different symmetry closely resembling each other. To understand this, consider first a semiclassical eigenfunction localized around $\psi_b = 0$, that is, a state that has nearly zero amplitude near $\psi_b = \pi$. Because the accessible configuration space is restricted to the vicinity of $(\psi_a, \psi_b) = (0, 0)$ for the lowest energies in the polyad, all eigenstates in this energy region fulfill this condition. First, the symmetry property in eq 57 implies that any semiclassical eigenfunction must be either symmetric or antisymmetric about $\psi_b = 0$. This symmetry reflects the parity of the eigenstate. In the context of states localized around $\psi_b = 0$, those states with an even number n_b have positive parity, and states with odd n_b have negative parity. The symmetry property of eq 58 implies that the wave function must be symmetric or antisymmetric with respect to a shift of 2π along ψ_b. This operation reflects the g/u symmetry. Thus, if a state has negligible amplitude near $\psi_b = \pi$, then it must appear in a doublet with a state of opposite g/u symmetry, that is, a state with nearly identical density but different signs at $\psi_b = 0$. If the state is mostly organized around $\psi_b = 0$ but has nonnegligible density in the vicinity of $\psi_b = \pi$, then the doublet pairs will split in a manner analogous to tunneling in a double well potential.

Similar arguments can be given for states localized about $\psi_b = \pi$, which includes all states at the energetic upper end of the polyad. Note that reflection about the line $\psi_b = \pi$ is equivalent to the application of both symmetry operations of eqs 57 and 58 in any order. As a result, states with an even n_b must have either g^+ or u^- symmetry. Those states with an odd n_b must be either g^- or u^+. As long as the states in question have little probability near $\psi_b = 0$ they appear in doublets of g^+/u^- or g^-/u^+.

The lift is now applied to determine the classical motion in displacement space that is quantized to produce the ladders. Clearly LB, CB, and CR states have point organizing centers as $(0, 0)$, $(0, \pi)$, and (π, π), respectively. For these, J_a and J_b

TABLE 4: Classification and Assignment of All States of Polyad $N_b = 22$, $L = 0$ of Acetylene[a]

label	energy	class	n_a	n_b
g+1	13926	LB	0	0
u+1	13926	LB	0	0
g-1	13985	LB	0	1
u-1	13985	LB	0	1
g+2	14036	LB	0	2
u+2	14036	LB	0	2
g+3	14064	LB	1	0
u+3	14064	LB	1	0
g-2	14081	LB	0	3
u-2	14081	LB	0	3
g+4	14120	LB	0	4
u+4	14120	LB	0	4
u-3	14136	LB	1	1
g-3	14136	LB	1	1
g-4	14153	LB	0	5
u-4	14153	LB	0	5
g+5	14181	LB	0	6
		(CB)	0	4
u+5	14181	LB	0	6
g+6	14188	LB	2	0
u+6	14188	LB	2	0
g+7	14197	LB	1	2
u+7	14197	LB	1	2
u-5	14200	CB	0	4
		(LB)	0	7
g-5	14205	CB	0	3
		(LB)	0	7
g+8	14213	CB	0	2
		(LB)	0	8
u+8	14226	CB	0	3
		(LB)	0	8
u-6	14228	CB	0	2
		(LB)	0	9
g-6	14241	LB	1	3
u-7	14241	LB	1	3
g-7	14249	CB	0	1
		(LB)	0	9
g+9	14250	CB	0	0
		(LB)	0	10
u+9	14275	CB	0	1
		(LB)	0	10
u-8	14275	CB	0	0
		(LB)	0	11
g+10	14281	LB	1	4
u+10	14281	LB	1	4
g-8	14282	LB	2	1
u-9	14282	LB	2	1
g+11	14311	LB	3	0
u+11	14311	LB	3	0
g-9	14316	LB	1	5
u-10	14316	LB	1	5
		(CB)	1	4
g+12	14336	LB	2	2
u+12	14336	LB	2	2
g+13	14344	LB	1	6
		(CB)	1	4
u+13	14344	LB	1	6
g-10	14365	LB	1	7
		(CB)	1	3
u-11	14366	LB	1	7
g+14	14378	CB	1	2
		(LB)	1	8
u+14	14383	CB	1	1
		(LB)	1	8
u-12	14386	LB	2	3
g-11	14387	LB	2	3
u-13	14390	CB	1	0
		(LB)	1	9
g-12	14390	CB	1	1
		(LB)	1	9
g+15	14393	CB	1	0
		(LB)	1	10
u+15	14418	LB	2	4
g+16	14419	LB	2	4
g-13	14425	LB	3	1
u-14	14425	LB	3	1
g+17	14429	LB	4	0
u+16	14430	LB	4	0
u-15	14456	LB	2	5
		(CB)	2	4
g-14	14460	LB	2	5
		(CB)	2	3
g+18	14460	LB	3	2
u+17	14461	LB	3	2
u+18	14470	LB	2	6
		(CB)	2	3
g+19	14486	CB	2	2
		(LB)	2	6
u-16	14493	CB	2	0
		(LB)	2	7
u+19	14513	CB	2	1
g-15	14514	CB	2	1
g+20	14515	LB	3	4
g-16	14520	LB	3	3
u-17	14522	LB	3	3
u-17	14522	(CB)	3	4
u+20	14531	CR	3	5
g+21	14537	CB	2	0
u-18	14538	CB	2	0
u+21	14550	CR	2	5
g+22	14552	CR	3	4
		(LB)	4	2
g-17	14568	LB	4	1
		(CR)	1	5
u-19	14571	LB	4	1
		(CR)	0	6
g-18	14574	CR	1	5
		(CB)	3	3
g+23	14578	CB	3	2
		(LB)	3	4
u+22	14578	LB	5	0
		(CR)	1	5
g+24	14586	LB	5	0
		(CR)	4	2
u-20	14596	CR	5	2
		(CB)	3	2
		(LB)	3	5
u+23	14613	CR	4	3
		(CB)	4	3
u+24	14621	CB	3	1
g-19	14632	CB	3	1
		(CR)	6	1
g+25	14642	CR	4	2
		(LB)	5	2
u-21	14645	CR	2	4
g-20	14658	CR	3	3
g+26	14663	CB	3	0
g+27	14664	CR	5	2
u-22	14670	CB	3	0
		(CR)	7	0
u+25	14674	CR	3	3
u-23	14699	CR	4	2
		(CB)	4	2
u+26	14704	CR	6	1
		(CB)	4	1
g+28	14719	LB	6	0
		(CR)	1	4
g-21	14722	CR	0	5
		(LB)	5	1
u-24	14725	CR	1	4
u+27	14725	CR	0	5
		(LB)	6	0
g+29	14740	CR	4	2
g-22	14743	CR	5	1
		(CB)	4	1
g+30	14755	CB	4	0
		(CR)	7	0
u+28	14774	CR	2	3
g-23	14777	CR	2	3
u-25	14789	CB	4	0
		(CR)	6	0
u+29	14797	CR	5	1
		(CB)	5	1
u-26	14806	CR	3	2
g+31	14812	CR	3	2
g+32	14851	CR	6	0
		(CB)	5	0
g-24	14853	CR	4	1
u+30	14875	CR	4	1
u+31	14891	CR	1	3
g+33	14883	CR	0	4
u-27	14883	CR	0	4
g-25	14889	CR	1	3
u-28	14907	CR	5	0
		(CB)	5	0
u-29	14929	CR	2	2
g+34	14930	CR	2	2
g+35	14954	CR	5	0
g-26	14971	CR	3	1
u+32	14974	CR	3	1
u-30	15026	CR	4	0
g+36	15040	CR	4	0
u+33	15054	CR	0	3
g-27	15054	CR	0	3
g+37	15068	CR	1	2
u-31	15068	CR	1	2
u+34	15107	CR	2	1
g-28	15107	CR	2	1
u-32	15157	CR	3	0
g+38	15158	CR	3	0
g+39	15240	CR	0	2
u-33	15240	CR	0	2
u+35	15264	CR	1	1
g-29	15264	CR	1	1
g+40	15307	CR	2	0
u-34	15307	CR	2	0
u+36	15446	CR	0	1
g-30	15446	CR	0	1
g+41	15478	CR	1	0
u-35	15478	CR	1	0
g+42	15672	CR	0	0
u-36	15672	CR	0	0

[a] First column gives the label of the states ordered by increasing energy. The second column gives the value of the energy in cm^{-1}. The third column gives the class into which the state is place. columns four and five give the two transverse quantum numbers. For many states, alternative classifications in different classes are possible. Therefore, we first give the most natural or obvious classification and quantum numbers and second give in the line below the alternative class (in parentheses) and the corresponding alternative quantum numbers. Note that for most sets of quantum numbers there are two states with the same set of quantum numbers coming from different symmetry representations, which form a doublet pair. The label of each state consists first of the symmetry representation to which it belongs (one of the four possibilities g+, g−, u+, or u−) and then a number which orders states within the symmetry representation according to increasing energy.

are obtained from eq 28 and $J_3 = K_a$ and $J_4 = K_b$. The values of ψ_a and ψ_b are the constant values of the point center, and θ_a and θ_b are obtained as functions of time from eq 29. Equation 55 now determines the matrix $\mathbf{M}$ in $\psi = (\mathbf{M}^{-1})^T \phi$; inverting gives $\phi(t)$, and from $I = \mathbf{M}^{-1} J$ we get $I(t)$. Equation 30 is needed to get position and momentum of the jth mode in terms of $I(t)$ and $\phi(t)$ obtaining the time dependence of the mode displacement and momentum variable. Conversion to Cartesian variables gives the atomic motion presented by illustrations in Figure 10. The origins of the LB, CB, and CR names are now evident.
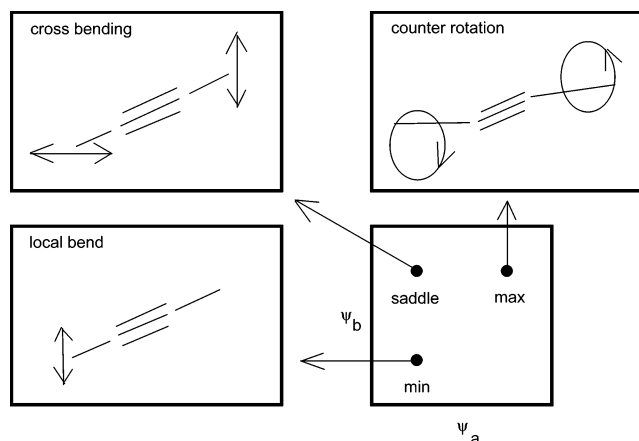
Angular momentum is conserved in all motions because of the fact that at any given time the trajectories of an opposite end of the molecule run in an opposite direction (straight lines under high diagrammatic resolution are long narrow figure-eight-like motions).

The polyad $N_b = 22$ sits astride the barrier, and the excitation of the LB class should lead to isomerization probably favoring the formation of vinylidene scissor modes or any other mode with a motion that when excited could go toward acetylene over the barrier and become an LB state. Isomerization theories that might use density of state arguments should consider using not the total density of states for acetylene at the barrier but that of the LB states.

Initial conditions for the trajectories that isomerize in either direction might actually be hard to find because of the stringent restriction of having to begin or end in phase space in regions

Extracting Dynamics from Spectroscopic Hamiltonians

J. Phys. Chem. A, Vol. 111, No. 16, 2007 **3067**

Figure 10. Illustration of the hydrogen motion belonging to the three important point organization centers of the bend dynamics of acetylene.

where LB states and scissor states exist respectively with the correct angular momentum direction for isomerization.

On the basis of motions that lead to isomerization, LB states should isomerize faster than CB states which in turn are faster than CR states. As such, when the barrier is exceeded and the total density of states increases, in analogy to scattering resonances, low-resolution spectra might well observe more CR than CB states and observe definitely more CR than LB states which have isomerized.

Interestingly, in 2005, Prosmiti and Farantos[46] re-examined their 1995 study[47] where they performed a numerical periodic orbit search on a six-dimensional potential energy surface of C_2H_2 (published in ref 19) and confirmed again that a CR mode develops out of a bifurcation of the cis bend periodic orbits and a local mode periodic orbit develops out of the trans bend periodic orbit.

The definitive classical work so far was done by Tyng and Kellman[48] in reduced (J, ψ) space with the same Hamiltonian as that used here. The evolution of the transition from cis and trans modes to that of CR and LB, respectively, along with the appearance of periodic orbits underlying the LB (0, 0), CB (0, π), and CR (π, π) organizing points were carefully tracked. All of this elegant work is consistent with our present approach and our first paper[1] where, in using nonlinear classical ideas supported by numerical estimations, it was observed that resonances set in at the K_a values at which cis and trans converts to CR and LB, respectively. CB was also found in ref 1. In ref 48 it was called the "orthogonal" mode. The precessional mode of ref 48 was not seen in ref 1 nor is it seen imprinted on any wave functions. This may mean that its region of influence is not large enough in units of $\hbar$ to support states.

Since ref 1 was published, two group theoretical approaches, refs 49 and 50, have been published. The first carried out a coset semiclassical analysis and confirmed the existence of local modes at the bottom and CRs at the top of the polyad as what appeared in ref 1. Other than the lowest states being local and the highest states being CRs, no immediate state dynamics and no assignment were made.

Using Lie algebraic methods, authors of ref 50 concluded that the majority of the states at the bottom and top of the polyad were local and CRs, respectively. Interestingly, they found 15 types of ideal bending modes and showed that many of the 144 states in polyad 22 could be associated with the 15 types. Eigenstates in polyad 22 were assigned using two global numbers and, as we do, N_b and L. How these quantum numbers are associated to the quantum numbers as represented by the organizing points given here which lift to periodic orbits in

normal mode space was an admitted open question and was deferred to a later paper which never appeared. The global quantum numbers are clearly associated with abstract unphysical operators that reveal little dynamics.

Authors of reference 51, using values of diagonal matrix elements of the various resonances, also came to conclusions similar to those of ref 49. Using advanced methods of scaling or so-called morphing coordinates of a superior potential surface for C_2H_2[52] and advanced methods for computing vibrational states, Xu et al. in ref 19 graphically exhibit the rigorously calculated highest and lowest states of polyad 16 to reveal their CR and LB nature. Since the work has produced all 144 eigenstates in displacement space, it is of interest to see if their full dimension wave functions can yield both dynamics and assignment.

12. Conclusion

The work covered here aims to start with a Hamiltonian fitted to experiment or equivalently to quantum chemically calculated vibrational level energies and aims to convert the problem of assignment and of uncovering the dynamics upon which the levels are quantized to one of wave function inspection in a semiclassical reduced dimension representation. It thus avoids all but the most trivial quantum or classical computation. The lessons of classical nonlinear dynamics are needed but the necessity to numerically study phase space or to seek periodic orbits is avoided.

Here, we have demonstrated that the simplified methodology reviewed in the previous sections opens new opportunities for gaining physical insights once the important interactions underlying complex multiresonant spectra have been uncovered by the presentation of a spectroscopic Hamiltonian. This insight was previously elusive because the very concept of multiple ladders or classes of differently organized states was not commonly used, and the idea that spectral complexity was due to anharmonic effects and the interleaving ladders and classes was not previously realized.

Previous analysis generally fell into several categories. Those that used classical or quantum Hamiltonians or even a spectral Hamiltonian in full dimension in configuration space were doomed to have only limited successes, at best, because of the "complexity" of trajectories, periodic orbits, wave functions, spectra, etc. Some extremely simple states like those most localized at the end of polyads and some simple periodic orbits might be spotted, but in general, no trends and no basic dynamics could be uncovered. This was true of methods that looked at eigenstates or at classically or quantum mechanically propagated wave packets. Full dimensional trajectories are generally too complicated to analyze. The very concept of using wave packets in the complex spectral region with the hope of getting dynamic insight is troubling to these authors. We now know that any initial packet would encompass many eigenstates of totally different dynamics that when used to evaluate the propagator would lead to recurrence patterns that mirror interferences which arise from the different dynamics and hence could be complicated and difficult to interpret. Packets can be run, and they could produce results in agreement with or predictive of experiments of energy transfer; however, the ability to extract any useful detailed information on the dynamics is, to us, generically unlikely unless technology allows the creation of a packet made of states on a single ladder. If this could be done for acetylene, that is, to create a packet of LB near barrier tunneling states, isomerization might be observable.

From the dynamical and semiclassical quantum point of view, the cause of these difficulties for studies of multiresonant

systems was the inability to take full advantage of the exact and approximate polyad constants of the motion for dimension reduction. This was impossible for the usual Schroedinger configuration space Hamiltonian and was an ignored simplification in many studies using spectroscopic Hamiltonians. These studies did not realize the great disadvantage of not reducing dimensions. First, a higher dimension is generally more complicated to view because the dynamics determining structures in reduced dimension, as organizing points, lines, or planes, repeats itself in the full dimension in a continuum of copies belonging to various values of the cyclic angles. For example, a simple line in reduced space could become a multidimensional torus in displacement and configuration space. Worse, because fixed polyad values are ignored, the effect of a continuous variation of conserved quantities cannot be avoided with the result that there are whole intervals of values of the conserved quantities where everything is the same with only very slight deformations.

To our knowledge, no prior work was able to uncover the full range of dynamically based assignments as done here. A similar statement holds for the dynamics itself. The concept of interleaving classes of states based on simple dynamics was not used before for multiresonant Hamiltonians that could exhibit large scale chaos.

The method has clear limits. Systems for which the reduced dimension is greater than three will make the viewing of wave functions difficult. For multiwell systems, the concept of a spectral Hamiltonian is challenged, and therefore, an analogous Hamiltonian does not exist. The problem but not the answer is seen from the fact that, for example for two well systems, two sets of action/angle variables, could be defined, and relating them is definitely a great challenge.

References and Notes

(1) Jacobson, M.; Jung, C.; Taylor, H. S.; Field, R. W. *J. Chem. Phys.* **1999**, *111*, 600.

(2) Jung, C.; Taylor, H. S.; Jacobson, M. P. *J. Phys. Chem. A* **2001**, *105*, 681.

(3) Temsamani, M. A.; Herman, M.; Solina, S. A.; O'Brien, J. P.; Field, R. W. *J. Chem. Phys.* **1996**, *105*, 11357.

(4) El Idrini, M. I.; Lievin, J.; Campargue, A.; Herman, M. *J. Chem. Phys.* **1999**, *110*, 2074.

(5) Jonas, D. M.; Solina, S. A. B.; Rajaram, B.; Cohen, S. J.; Field, R. W.; Yamanouchi, K.; Tsuchiya, S. *J. Chem. Phys.* **1993**, *99*, 7350.

(6) Jacobson, M. P.; O'Brien, J. P.; Silbey, R. J.; Field, R. W. *J. Chem. Phys.* **1998**, *109*, 121.

(7) Jung, C.; Ziemniak, E. M.; Taylor, H. S. *J. Chem. Phys.* **2001**, *115*, 2499.

(8) Beil, A.; Luckhaus, D.; Quack, M. *Mol. Phys.* **1995**, *56*, 727. Beil, A.; Luckhaus, D.; Quack, M.; Stohner, J. *Ber. Bunsen–Ges.* **1997**, *100*, 1853. Beil, A.; Luckhaus, D.; Marquardt, R.; Quack, M. *J. Chem. Soc., Faraday Trans.* **1994**, *99*, 49.

(9) Jung, C.; Taylor, H. S.; Atilgan, E. *J. Phys. Chem. A* **2002**, *106*, 3092.

(10) Troellsch, A.; Temps, F. *Z. Phys. Chem.* **2001**, *215*, 207.

(11) Jung, C.; Mejia-Monasterio, C.; Taylor, H. S. *J. Chem. Phys.* **2004**, *120*, 4194.

(12) Beil, A.; Hollenstein, H.; Monti, O. L. A.; Quack, M.; Stohner, J. *J. Chem. Phys.* **2000**, *113*, 2701.

(13) Jung, C.; Mejia-Monasterio, C.; Taylor, H. S. *Phys. Chem. Chem. Phys.* **2004**, *6*, 3069.

(14) Pochert, J.; Quack, M.; Stohner, J.; Willeke, M. *J. Chem. Phys.* **2000**, *113*, 2719.

(15) Jung, C.; Taylor, H. S.; Sibert, E. L. *J. Phys. Chem. A* **2006**, *110*, 5317.

(16) Bigwood, R.; Millan, B.; Gruebele, M. *Chem. Phys. Lett.* **1998**, *287*, 333.

(17) Herzberg, G. *Infrared and Raman Spectra of Polyatomic Molecules;* Van Norstrand Reinhold: New York, 1945.

(18) Bramley, M. J.; Carrington, T. *J. Chem. Phys.* **1994**, *101*, 8494.

(19) Xu, D.; Guo, H.; Zou, S.; Bowman, J. M. *Chem. Phys. Lett.* **2003**, *377*, 582.

(20) Xu, D.; Chen, R.; Guo, H. *J. Chem. Phys.* **2003**, *118*, 7273.

(21) Mandelshtam, V. A.; Grozdanov, T. P.; Taylor, H. S. *J. Chem. Phys.* **1995**, *103*, 10074.

(22) Jacobson, M. P.; Silbey, R. J.; Field, R. W. *J. Chem. Phys.* **1999**, *110*, 845.

(23) Zuniga, J.; Bastida, A.; Requena, A.; Sibert, E. L. *J. Chem. Phys.* **2002**, *116*, 7495.

(24) Fried, L. E.; Ezra, G. *J. Chem. Phys.* **1987**, *86*, 6270.

(25) Joyeaux, M. *Chem. Phys.* **1994**, *185*, 263.

(26) Kellman, M. E. *J. Chem. Phys.* **1990**, *93*, 6630.

(27) Heisenberg, W. *Z. Phys.* **1925**, *33*, 879.

(28) Grey, S.; Child, M. S. *Mol. Phys.* **1984**, *53*, 961.

(29) Sibert, E. L.; Hynes, J. T.; Reinhard, W. P. *J. Chem. Phys.* **1982**, *77*, 3583.

(30) Sibert, E. L.; McCoy, A. B. *J. Chem. Phys.* **1996**, *105*, 469.

(31) Keshavamurthy, S.; Ezra, G. S. *Chem. Phys. Lett.* **1996**, *259*, 81.

(32) Keshavamurthy, S.; Ezra, G. S. *J. Chem. Phys.* **1997**, *107*, 156.

(33) Lu, Z.; Kellman, M. E. *Chem. Phys. Lett.* **1995**, *247*, 195.

(34) Rose, J. P.; Kellman, M. E. *J. Chem. Phys.* **1996**, *105*, 7348.

(35) Lawton, R. T.; Child, M. S. *Mol. Phys.* **1980**, *40*, 773.

(36) Stamatiadis, S.; Farantos, S. C.; Keller, H. M.; Schinke, R. *Chem. Phys. Lett.* **1999**, *311*, 2416.

(37) Hose, G.; Taylor, H. S. *Phys. Rev. Lett.* **1983**, *51*, 947.

(38) Brack, M.; Bhaduri, R. K. *Semiclassical Physics;* Addison Wesley: Reading, MA, 1997.

(39) Jackson, E. A. *Perspectives of Nonlinear Dynamics;* Cambridge University Press: Cambridge, U.K., 1991.

(40) Gutzwiller, M. C. *Chaos in Classical and Quantum Mechanics;* Springer-Verlag: New York, 1990.

(41) Lichtenberg, A.; Liberman, M. *Regular and Stochastic Motion*, Springer-Verlag: New York, 1983.

(42) Chirikov, B. *Phys. Rep.* **1979**, *52*, 263.

(43) Rueda, J.; Jung, C. *Mol. Phys.* **2006**, *104*, 1353.

(44) Cohen-Tannoudji, C.; Dieu, B.; Laloë, F. *Quantum Mechanics;* John Wiley and Sons: New York, 1977.

(45) van Ede van der Pals, P.; Gaspard, P. *J. Chem. Phys.* **1999**, *110*, 5619.

(46) Prosmiti, R.; Farantos, S. C. *J. Chem. Phys.* **2003**, *118*, 8275.

(47) Prosmiti, R.; Farantos, S. C. *J. Chem. Phys.* **1995**, *103*, 3299.

(48) Tyng, V.; Kellman, M. E. *J. Phys. Chem. B* **2006**, *110*, 18859.

(49) Yu, J.; Wu, G. *J. Chem. Phys.* **2000**, *113*, 647.

(50) Chamrion, J. M.; Abbouti Temsamani, M.; Oss, S. Quantum representations of dynamical systems: new bending modes of acetylene. *PhysChemComm.* 2000, *3*, article 2. http://www.rsc.org/Publishing/Journals/QU/articles.asp?doi=b001934h.

(51) Semparithi, A.; Keshavamurthy, S. *Chem. Phys. Lett.* **2004**, *395*, 327.

(52) Zou, S.; Bowman, J. M. *Chem. Phys. Lett.* **2003**, *386*, 421.